HHS Public Access

Author manuscript

Cell Rep. Author manuscript; available in PMC 2021 January 12.

Published in final edited form as:

Cell Rep. 2020 November 17; 33(7): 108365. doi:10.1016/j.celrep.2020.108365.

Coupled Control of Distal Axon Integrity and Somal Responses to Axonal Damage by the Palmitoyl Acyltransferase ZDHHC17

Jingwen Niu[1,7], **Shaun S. Sanders**[1,7], **Hey-Kyeong Jeong**[1,7], **Sabrina M. Holland**[1], **Yue Sun**[2], **Kaitlin M. Collura**[1], **Luiselys M. Hernandez**[1], **Haoliang Huang**[3], **Michael R. Hayden**[4], **George M. Smith**[1,5], **Yang Hu**[3], **Yishi Jin**[2], **Gareth M. Thomas**[1,6,8,*]

[1]Shriners Hospitals Pediatric Research Center, Lewis Katz School of Medicine at Temple University, 3500 N. Broad Street, Philadelphia, PA 19140, USA

[2]Section of Neurobiology, Division of Biological Sciences, University of California, San Diego, La Jolla, CA 92093, USA

[3]Department of Ophthalmology, Stanford University School of Medicine, Palo Alto, CA 94304, USA

[4]Department of Medical Genetics, Centre for Molecular Medicine and Therapeutics, University of British Columbia, Vancouver, BC, Canada

[5]Department of Neuroscience, Lewis Katz School of Medicine at Temple University, Philadelphia, PA 19140, USA

[6]Department of Anatomy and Cell Biology, Lewis Katz School of Medicine at Temple University, Philadelphia, PA 19140, USA

[7]These authors contributed equally

[8]Lead Contact

SUMMARY

After optic nerve crush (ONC), the cell bodies and distal axons of most retinal ganglion cells (RGCs) degenerate. RGC somal and distal axon degenerations were previously thought to be controlled by two parallel pathways, involving activation of the kinase dual leucine-zipper kinase (DLK) and loss of the axon survival factor nicotinamide mononucleotide adenylyltransferase-2 (NMNAT2), respectively. Here, we report that palmitoylation of both DLK and NMNAT2 by the palmitoyl acyltransferase ZDHHC17 couples these signals. ZDHHC17-dependent palmitoylation enables DLK-dependent somal degeneration after ONC and also ensures NMNAT-dependent distal axon integrity in healthy optic nerves. We provide evidence that ZDHHC17 also controls survival-

*Correspondence: gareth.thomas@temple.edu.

AUTHOR CONTRIBUTIONS

Conceptualization, Supervision, and Funding Acquisition, G.M.S., Y.H., Y.J., and G.M.T.; Investigation, J.N., S.S.S., H.-K.J., S.M.H., Y.S., K.M.C., L.H., and G.M.T.; Methodology, H.H., Y.H., and G.M.T.; Resources, M.R.H. and G.M.S.

SUPPLEMENTAL INFORMATION

Supplemental Information can be found online at https://doi.org/10.1016/j.celrep.2020.108365.

DECLARATION OF INTERESTS

The authors declare no competing interests.

versus-degeneration decisions in dorsal root ganglion (DRG) neurons, and we identify conserved motifs in NMNAT2 and DLK that govern their ZDHHC17-dependent regulation. These findings suggest that the control of somal and distal axon integrity should be considered as a single, holistic process, mediated by the concerted action of two palmitoylation-dependent pathways.

Graphical Abstract

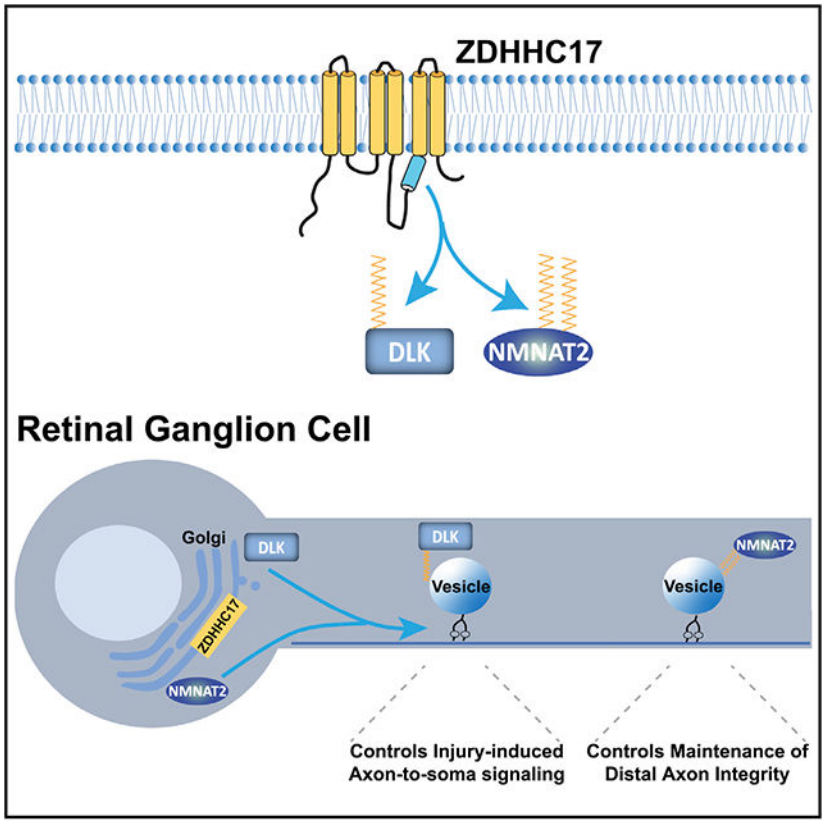

In Brief

Niu et al. show that ZDHHC17 palmitoylates DLK, a mediator of axon-to-soma pro-degenerative signaling, and also NMNAT2, a survival factor whose rapid loss post-injury triggers distal axon degeneration. Palmitoylation of these two key proteins by ZDHHC17 ensures a coordinated response of distal axons and neuronal somas to axonal injury.

INTRODUCTION

Retinal ganglion cells (RGCs) are thought to undergo compartmentalized cell death after axonal injury, with different pathways controlling degeneration of the RGC soma and distal axons. This model emerged from findings that knockout (KO) of the proapoptotic protein Bax strongly protects RGC somas, but not distal axons after optic nerve crush (ONC), whereas the *Wld*^{S} (*Wallerian degeneration slow*) spontaneous mutation protects distal axons, but not RGC somas (Howell et al., 2013; Li et al., 1999, 2000; Libby et al., 2005).

Since those initial findings, more is now known about pathways that trigger somal Bax activation and how *Wld*^{S} protects axons. Bax lies downstream of a mitogen-activated protein kinase (MAPK) pathway involving dual leucine-zipper kinase (DLK) and DLK's direct targets MKK4/MKK7, which in turn activate c-Jun N-terminal kinase (JNK) (Fernandes et al., 2012, 2014; Maes et al., 2017; Watkins et al., 2013; Welsbie et al., 2013, 2017). The DLK-JNK pathway is thought to convey an axon-to-soma signal, resulting in phosphorylation of transcription factors, most notably c-Jun, and upregulation of pro-apoptotic genes that then activate Bax (Watkins et al., 2013). Like *Bax* KO, DLK KO strongly protects RGC somas post-ONC but protects distal RGC axons minimally, if at all (Fernandes et al., 2014; Yang et al., 2015).

In diverse neuron types, continuous anterograde transport of the labile biosynthetic enzyme nicotinamide mononucleotide adenylyltransferase-2 (NMNAT2) maintains axon integrity (Coleman and Freeman 2010; Gilley and Coleman 2010; Yamagishi and Tessier-Lavigne, 2016). Axonal injury interrupts this transport, and rapid loss of remaining NMNAT2 in the severed distal axon triggers Wallerian degeneration (Gerdts et al., 2016). The *Wld*^{S} protein (an unnatural, stable form of NMNAT2's paralog NMNAT1) or a cytosolic form of NMNAT1 (cytoNMNAT1) (Yang et al., 2015) strongly protects RGC distal axons post-injury, likely by substituting for NMNAT2 (Fernandes et al., 2014; Lorber et al., 2012). KO of SARM1 (Fernandes et al., 2018; Yang et al., 2015), an "axon executioner" enzyme that is activated downstream of NMNAT2 loss (Gilley et al., 2015, 2017) also blocks ONC-induced axon degeneration, but neither *Wld*^{S} nor SARM1 KO prevent ONC-induced RGC somal loss (Beirowski et al., 2008; Fernandes et al., 2014, 2018; Lorber et al., 2012).

The above DLK-JNK and NMNAT2-SARM1 studies support the compartmentalized RGC death model. However, we hypothesized that these pathways may be coordinated, based on findings that both DLK and NMNAT2 localize to axonal vesicles and that their vesicle targeting involves the same mechanism–palmitoylation. This protein-lipid modification is essential for vesicular trafficking of both DLK and NMNAT2 in cultured neurons (Holland et al., 2016; Milde et al., 2013). However, the importance of palmitoylation of DLK and NMNAT2 in the optic nerve *in vivo* and the palmitoyl acyltransferase (PAT) responsible are unknown.

Here, we use adeno-associated virus (AAV)-mediated molecular replacement to define the importance of DLK and NMNAT2 palmitoylation for RGC somal and distal axon integrity *in vivo*. We first show that DLK palmitoylation is critical for ONC-induced axon-to-soma signaling and subsequent RGC somal degeneration. We then identify the PAT ZDHHC17 as an evolutionarily conserved regulator of DLK palmitoylation and signaling. We further show that DLK and NMNAT2 palmitoyl sites are homologous and provide evidence that ZDHHC17-dependent palmitoylation of NMNAT2 is essential for distal axon integrity in cultured neurons and *in vivo*. These results provide unexpected insights into the control of DLK and NMNAT2 signaling and increase our understanding of how somal and distal axon degeneration are coupled and controlled.

RESULTS

Palmitoyl-DLK Is Essential for RGC Somal Responses to Axon Injury

We first used genetic manipulation, mediated by intravitreal AAV delivery (Martin et al., 2002; Figure 1A), to ask whether DLK palmitoylation is necessary for RGC somal responses to ONC. In uninfected wild-type (WT) mice, ONC greatly increased phosphorylation of c-Jun (P-c-Jun) in RGCs and decreased levels of Brn3a, a marker of healthy RGCs, as in prior studies (Figure S1A; Fernandes et al., 2014; Watkins et al., 2013; Welsbie et al., 2013, 2017). ONC also increased levels of P-c-Jun and DLK in retinas that had been intravitreally infected with control (GFP-expressing) AAV (Figures 1B, 1C, S1B, and S1C). However, ONC-induced P-c-Jun and DLK increases were prevented in retinas infected with AAV expressing GFP plus DLK short hairpin RNA (shRNA) (AAV-GFP-DLKsh; Figures 1B, 1C, S1B, and S1C), similar to prior work (Watkins et al., 2013; Welsbie et al., 2013).

DLK's Cys127 palmitoylation site is critical for DLK localization and function in cultured neurons (Holland et al., 2016). To address the importance of DLK palmitoylation in somal responses to ONC, we coinfected retinas with AAV-GFP-DLKsh and a second AAV expressing hemagglutinin (HA)-tagged shRNA-resistant forms of either WT or palmitoyl mutant (Cys127Ser: "CS") DLK (AAV-WT-DLK*-HA, AAV-DLK-CS*-HA; "WT*" and "CS*" in Figure 1B). WT-DLK*-HA, but not DLK-CS*-HA, restored ONC-induced P-c-Jun to WT levels (Figures 1B and 1C). WT-DLK*-HA and DLK-CS*-HA expressed at similar levels (Figure 1B) and in a similar fraction of GFP-positive neurons (Figure S1D).

We next used RNA-binding protein with multiple splicing (RBPMS), an RGC marker whose expression is unaffected by ONC (Kwong et al., 2011), to assess RGC somal viability at 3 weeks post-ONC (Figures 1A and 1D). ONC greatly reduced RGC counts in AAV-GFP-infected, but not AAV-GFP-DLKsh-infected, retinas (Figures 1D and 1E), similar to prior studies (Fernandes et al., 2014; Watkins et al., 2013; Welsbie et al., 2013). AAV-WT-DLK*-HA, but not AAV-DLK-CS*-HA, rescued ONC-induced RGC loss (WT* and CS*; Figures 1D and 1E). In uninjured retinas, WT-DLK*-HA slightly increased P-c-Jun but did not reduce RGC viability (Figures 1C and 1E). AAV also sparsely infected RBPMS-negative cells (Figure 1D), likely displaced amacrine cells (Perry 1981), but these were not included in RGC viability analyses. These data suggest that RGC somal responses to ONC require palmitoyl-DLK.

The PAT ZDHHC17 Is an Evolutionarily Conserved DLK Regulator

The expression of >20 of the 24 mammalian PATs in RGCs (Sajgo et al., 2017; Tran et al., 2019) potentially complicates identification of the PAT(s) that palmitoylates DLK. As CS mutation shifts localization of DLK orthologs from membrane associated to diffuse in HEK293T cells and also in rodent and *C. elegans* sensory neurons (Holland et al., 2016; Martin et al., 2019), we reasoned that the DLK PAT should be evolutionarily conserved. The most conserved PAT is ZDHHC17, which, unlike most PATs, has six rather than four predicted transmembrane domains (TMDs), plus an N-terminal ankyrin repeat (AnkR) region, in addition to the enzymatic DHHC (Asp-His-His-Cys) domain (Figure 2A; Roth et

al., 2002; Young et al., 2012). Two *C. elegans* PATs, DHHC-13 and DHHC-14 (Edmonds and Morgan 2014), are presumptive ZDHHC17 orthologs (Figure 2A). Double KO of *dhhc-13* and *dhhc-14* shifted localization of a GFP-tagged *C. elegans* DLK ortholog (GFP-CeDLK-1) from punctate to diffuse (Figures 2B, 2C, and S2A), suggesting that ZDHHC17 orthologs regulate CeDLK-1.

ZDHHC17 Regulates DLK via AnkR-Mediated Binding

We next asked whether ZDHHC17 is a PAT for mammalian DLK. In cotransfected HEK293T cells, ZDHHC17 coimmunoprecipitated GFP-tagged WT-DLK (WT-DLK-GFP) more effectively than did six other candidate DLK PATs (Holland et al., 2016; Figure S2B). Of these PATs, only ZDHHC17 contains an AnkR, suggesting ZDHHC17 might bind DLK via this region. ZDHHC17's AnkR recognizes a ZDHHC ankyrin domain binding motif (zDABM; [AIPV][ITV]XX[CMQ][IP]X[KR]) in several ZDHHC17 substrates (Lemonidis et al., 2015, 2017). We identified a matching PVXXMIXK sequence close to DLK's palmitoylation site (Figure S2C). Mutating this zDABM (PV-AA mutant; Figure S2C) reduced DLK-GFP palmitoylation, assessed by acyl biotin exchange (ABE) assays. We previously reported that Golgi targeting of DLK-GFP in HEK293T cells is palmitoylation dependent (Martin et al., 2019), but the DLK PV-AA mutant showed reduced Golgi targeting and palmitoylation, even when ZDHHC17-HA was cotransfected (Figures S2D-S2G). Neither palmitoylation nor Golgi targeting of WT-DLK-GFP was increased by ZDHHC17-N100A, a mutant that poorly recognizes zDABM-containing substrates (Verardi et al., 2017; Figures S2D-S2G). These findings suggest that ZDHHC17 palmitoylates DLK in an AnkR-zDABM-dependent manner.

ZDHHC17 Controls Palmitoylation and Signaling of Endogenous Mammalian DLK

ZDHHC17 is highly expressed in RGCs (Sajgo et al., 2017; Tran et al., 2019), making it a strong candidate to palmitoylate endogenous DLK. However, isolating sufficient amounts of pure RGCs for ABE assays is difficult, so we addressed this question using cultured DRG neurons, in which somal responses to axon insult/injury also require DLK and its palmitoylation (Ghosh et al., 2011; Holland et al., 2016; Simon et al., 2016). DLK palmitoylation in DRG neurons (normalized to total DLK expression) was greatly reduced by *Zdhhc17* knockdown (Figures 2D-2F, S2H, and S2I). As a control, knockdown of *Zdhhc5* and *Zdhhc8*, two PATs that strongly palmitoylate DLK in non-neuronal cells (Holland et al., 2016), did not affect DLK palmitoylation (Figure S2J). *Zdhhc17* knockdown also reduced palmitoylation of JNK3, DLK's downstream target (Figure S2K), but did not affect palmitoylation of another axonal palmitoyl protein, GAP43 (Figures 2D-2F). These results suggest that ZDHHC17 is a major PAT for DLK in DRG neurons.

DLK-Dependent Somal Responses to Axonal Insult and Injury Require ZDHHC17

Does *Zdhhc17* loss prevent somal responses to axon insult or injury through the loss of palmitoyl-DLK? DRG neuron somal responses to trophic factor deprivation (TD) are DLK dependent (Ghosh et al., 2011; Simon et al., 2016), so we first asked whether such responses also require palmitoyl-DLK. TD increased P-c-Jun in DRG neuron somas and, over prolonged times, activated caspase-3, a key "commitment to die'' step, as in prior studies (Deshmukh et al., 2000; Ghosh et al., 2011; Simon et al., 2016; Figures S3A-S3D). Both P-

c-Jun increases and caspase-3 activation were prevented by DLKshRNA and rescued by WT-DLK*, but not DLK-CS* (Figures S3A-S3D). *Zdhhc17* knockdown also attenuated TD-induced P-c-Jun (Figures 3A and 3B), suggesting that pro-degenerative signaling in DRG neurons requires palmitoyl-DLK and ZDHHC17.

To address whether loss of ZDHHC17 phenocopies loss of palmitoyl-DLK *in vivo*, we intravitreally delivered AAV-GFP or AAV-Cre-T2A-GFP (expressing Cre recombinase linked via a self-cleaving T2A sequence to GFP) to *Zdhhc17*$^{f/f}$ mice (Sanders et al., 2016). After ONC, both P-c-Jun and active caspase-3 (a commitment to die step in RGCs, just as in DRGs; Sánchez-Migallón et al., 2016) were far less frequent in AAV-Cre-T2A-GFP-infected (i.e., *Zdhhc17* conditional KO [CKO]) retinas than in AAV-GFP-infected retinas (Figures 3C-3F). These findings suggest that ZDHHC17 palmitoylates DLK and that this post-translational modification is essential for somal responses to axonal injury/insult in DRG neurons and RGCs.

We also asked whether ZDHHC17 might palmitoylate DLK in other neuron types by analyzing single-cell RNA sequencing (RNA-seq) data (http://www.mousebrain.org; Zeisel et al., 2018). We found that DLK (gene name *Map3k12*) mRNA expression correlates better with *Zdhhc17* expression than with expression of any other PAT across 265 nervous system cell types (Figures S3E and S3F). Though correlative, these data suggest that ZDHHC17 may palmitoylate DLK in other neuronal types.

ZDHHC17 Binds and Palmitoylates NMNAT2

Several lines of evidence suggested that ZDHHC17 might also palmitoylate the axon survival factor NMNAT2. First, the DLK and NMNAT2 palmitoyl-site motifs are more similar to one another than to any other known palmitoyl site (Figure 4A; see STAR Methods for bioinformatic search details). Second, NMNAT2 also contains a predicted zDABM close to its palmitoyl motif (Figure 4B), and both regions are conserved in vertebrates (Figure 4B). Third, ZDHHC17 was implicated as a potential PAT for NMNAT2, based largely on findings in non-neuronal cells (Milde and Coleman, 2014).

We verified that, when expressed in HEK cells, ZDHHC17 robustly bound and palmitoylated cotransfected NMNAT2 (Figures S4A and S4B), consistent with Milde and Coleman (2014). In addition, ABE assays revealed that *Zdhhc17* knockdown markedly reduced NMNAT2 palmitoylation in DRG neurons (Figures 4C and 4D). *Zdhhc17* knockdown also reduced NMNAT2 total levels (but to a lesser extent than palmitoylation; Figures 4C and S4C), perhaps because NMNAT2 is unstable and may be degraded if targeted to the Golgi, but not palmitoylated. These findings suggest that ZDHHC17 is a major PAT for NMNAT2 in neurons.

We next asked whether NMNAT2's zDABM is important for palmitoylation by ZDHHC17. Mutation of NMNAT2's zDABM (NMNAT2-4A mutant) and ZDHHC17-N100A mutation both reduced NMNAT2 palmitoylation by ZDHHC17 (Figures S4D and S4E). Mutating 5 basic residues surrounding the palmitoyl motif also reduces NMNAT2 palmitoylation ("BR" mutant; Milde et al., 2013). Two of these 5 sites (R162 and R167) abut NMNAT2 palmitoyl sites (Figure 4B), and their mutation may affect NMNAT2 recognition by its PAT. However,

a more subtle NMNAT2-3BR mutant containing only 3 of 5 basic site mutations, distal from NMNAT2's palmitoyl sites was also less palmitoylated by ZDHHC17 than NMNAT2-WT, and a combination mutant (NMNAT2-4A-3BR) was even less palmitoylated (Figures S4D and S4E). These results suggest that DLK and NMNAT2 share similar palmitoyl sites and possess similar motifs that facilitate their palmitoylation by ZDHHC17.

We next asked whether these motifs control NMNAT2 localization in DRG neurons. Lentivirally expressed NMNAT2-WT-myc colocalized with the Golgi marker GM130 and was also detected on axonal puncta that are likely vesicles (Figure 4E), consistent with prior reports (Berger et al., 2005; Milde et al., 2013). NMNAT2-4A-3BR-myc (Figure 4B) expressed at similar levels to NMNAT2-WT-myc (Figures S4F and S4G) and still colocalized with GM130 but was much less detectable in axons (Figures 4E and 4F). These findings suggest that, as in non-neuronal cells (Figures S4D and S4E), the BR/zDABM combination controls neuronal NMNAT2 palmitoylation, which is in turn important for NMNAT2 axonal targeting.

To address whether ZDHHC17 might regulate NMNAT2 in other neuron types, we again analyzed RNA-seq data (http://www.mousebrain.org) and found, similar to DLK, that *Nmnat2* mRNA expression correlates better with *Zdhhc17* expression than with expression of any other PAT (Figures S4H and S4I). Though again correlative, these findings suggest that ZDHHC17 may palmitoylate NMNAT2 in other neuronal types.

We next asked where in the neuron ZDHHC17 might palmitoylate DLK and NMNAT2. Lentivirally expressed HA-ZDHHC17 was detected in DRG neuron somas, but not axons (Figure 4G). Similarly, endogenous ZDHHC17 was biochemically detected in somal, but not distal, axon fractions of DRG microfluidic cultures (Figures 4H and 4I). Tubulin and GAP-43 were detected in both somal and distal axon fractions, while histone H3 was only seen in somal fractions, supporting the fidelity of the preparation (Figure 4H). In the soma, HA-ZDHHC17 colocalized with GM130 (Figure 4J), consistent with studies from non-neuronal cells (Ernst et al., 2018; Ohno et al., 2006). These findings suggest that ZDHHC17 likely palmitoylates DLK and NMNAT2 on the somatic Golgi, consistent with transport of WT (i.e., palmitoylation-competent) DLK and NMNAT2 on Golgi-derived vesicles (Holland et al., 2016; Milde et al., 2013).

ZDHHC17 Is Essential for NMNAT-Dependent Distal Axon Integrity

We next addressed the functional role of NMNAT2 palmitoylation by ZDHHC17. NMNAT2 anterograde transport, which is palmitoylation-dependent, normally maintains axonal levels of nicotinamide adenine dinucleotide (NAD^+) to prevent distal axon degeneration (Gilley et al., 2015; Milde et al., 2013). We therefore asked whether loss of *Zdhhc17* phenocopies loss of *Nmnat2* to reduce axon integrity. Indeed, distal DRG axons in culture degenerated after prolonged *Zdhhc17* knockdown (Figures 5A-5C). Axon degeneration was reduced by either coinfected cytoNMNAT1 or by NAD^+ addition (Figures 5B and 5C). These approaches both compensate for endogenous NMNAT2 loss (Sasaki et al., 2006; Yang et al., 2015), suggesting that impaired NMNAT2 palmitoylation underlies axon degeneration induced by *Zdhhc17* loss (Sasaki et al., 2006; Wang et al., 2015).

Finally, we asked whether prolonged loss of *Zdhhc17* impacts distal axons via loss of palmitoyl-NMNAT2 supply *in vivo*. Intravitreal injection of *Zdhhc17*$^{f/f}$ mice with AAV-Cre-T2A-GFP, but not AAV-GFP, caused delayed degeneration of distal optic nerves 13 days later, assessed by axon fragmentation and microgliosis (Ebneter et al., 2010; Palin et al., 2008; Figures 5D-5F). RGC somal viability was unaffected at this time (Figures S5A and S5B), suggesting that loss of an axon-intrinsic factor likely underlies the degeneration and microgliosis. Consistent with this notion and with the phenotypic similarity to the NMNAT-dependent axon degeneration in DRG neurons, cyto-NMNAT1-HA reduced distal axon breakdown and microgliosis in *Zdhhc17* CKO optic nerves (Figures 5D-5F). Distal axon degeneration and microgliosis were even more evident 17 days after *Zddhc17* CKO and were still fully rescued by cytoNMNAT1-HA (Figures S5C and S5D). Proximal axons remained intact at this later time, although RGC somal viability was slightly reduced (Figures S5E-S5G). These results suggest that loss of endogenous NMNAT2 palmitoylation underlies distal axon degeneration in *Zdhhc17* CKO mice.

DISCUSSION

RGCs were thought to undergo compartmentalized degeneration post-injury, with DLK/JNK retrograde signals driving somal death and NMNAT2 loss triggering distal axon self-destruction. Although consistent with this model, our findings reveal that palmitoylation by the same PAT, ZDHHC17, couples the DLK and NMNAT2 signals, which act in concert to form an axonal “trust, but verify” system. We suggest that healthy RGCs supply palmitoyl-NMNAT2 to distal axons to signal that all is well but also supply palmitoyl-DLK to respond to axonal injury. After ONC, palmitoyl-DLK-dependent retrograde signals cause somal death, while interruption of palmitoyl-NMNAT2 anterograde transport triggers distal axon degeneration. This system thus ensures a coordinated response, even if injury prevents communication by electrical signaling or protein trafficking, between somas and distal axons.

Unanticipated Roles for ZDHHC17 in Acute Injury Signaling

ZDHHC17 was first named Huntingtin (HTT)-interacting protein-14 (Hip14) for its binding to the protein whose poly-glutamine expansion underlies Huntington disease (Singaraja et al., 2002). Mutant HTT reduces ZDHHC17 activity and prolonged, global *Zdhhc17* loss phenocopies several features of HD in mice (Huang et al., 2011; Singaraja et al., 2011). These findings suggest that ZDHHC17 is neuroprotective in the context of HD, and accordingly, ZDHHC17 can palmitoylate several regulators of physiological neuronal function (Huang et al., 2004). However, we identified key roles for ZDHHC17 in acute neurodegeneration (Figures 2 and 5). Factors that govern ZDHHC17 activity toward pro-survival versus pro-death substrates in different neuropathological conditions are worthy of investigation. Intriguingly, loss of NMNAT2 palmitoylation (and consequent NAD^+ loss) in motor axons may also explain the paralysis caused by *Zdhhc17* KO in adult mice (Sanders et al., 2016).

DLK and NMNAT2 Are Major ZDHHC17 Substrates Responsible for Somal and Distal Axon Integrity

ZDHHC17 has many potential substrates (Greaves et al., 2010; Huang et al., 2004), so to what extent can we ascribe our observed phenotypes to direct regulation of DLK and/or NMNAT2? Importantly, impaired DLK palmitoylation and axon-to-soma signaling are the most immediate effects of *Zdhhc17* loss, occurring when cell bodies and proximal axons of *Zdhhc17* CKO neurons are phenotypically normal (Figures 1, S5A, and S5E). Other ZDHHC17 substrates are thus unlikely to account for these phenotypes. *Zdhhc17* knockdown also reduces JNK3 palmitoylation, albeit to a lesser extent than that of DLK, raising the intriguing possibility that ZDHHC17 regulates both DLK and its downstream target JNK3. We cannot thus exclude a contribution of reduced JNK3 palmitoylation to ZDHHC17-dependent phenotypes, but to our knowledge, palmitoylation of JNK3 has not been linked to axonal pro-degenerative signaling, so impairments of such signaling after *Zddhc17* loss are more readily explained by effects on palmitoyl-DLK. A myristoylated DLK mutant ("Myr-DLK-CS") could potentially be used in *Zdhhc17* knockdown neurons to test this hypothesis, but Myr-DLK-CS palmitoylation at non-physiological sites (Holland et al., 2016) complicates this approach.

Distal axon degeneration occurs later after *Zdhhc17* loss, but RGC somal viability initially remains unaltered (Figures 5, S5A, and S5B), minimizing the likelihood of indirect effects. Moreover, ZDHHC17's best-known substrates SNAP25 and CSP are not linked to axon integrity to our knowledge (Fernández-Chacón et al., 2004; Washbourne et al., 2002), and loss of another ZDHHC17 substrate, HTT, triggers axon degeneration only in developing and not adult mice (Dragatsis et al., 2000; Wang et al., 2016). Most importantly, the axon degeneration is rescued by genetically or pharmacologically restoring levels of the NMNAT2 reaction product NAD^+ (Figures 5, S5C, and S5D). Although we cannot exclude roles of other ZDHHC17 substrate(s), NMNAT2 is thus likely the key substrate whose lack of palmitoylation triggers axon degeneration after *Zdhhc17* loss.

Golgi Localization of ZDHHC17 Is Critical for the Coupled Action of DLK and NMNAT2

ZDHHC17 could potentially regulate DLK and/or NMNAT2 more acutely if it were localized to distal axons, yet ZDHHC17 is confined to somatic Golgi-like membranes (Figure 4). This location is consistent with localization of WT (i.e., palmitoylation-competent) DLK and NMNAT2 to Golgi-derived vesicles (Holland et al., 2016; Milde et al., 2013) and also matches models of NMNAT2 action. In particular, NMNAT2 is essential to maintain axonal NAD^+ levels (Gilley et al., 2015), but NMNAT2 supply to distal axons is likely limiting, balanced by axonal NMNAT2 degradation (Gilley and Coleman 2010; Milde et al., 2013). Consistent with this model, distal axons degenerate first in dying back axonopathies (Coleman and Freeman 2010), in turn explaining the "stockings and gloves" pathology of such conditions (Argyriou et al., 2014). Significant NMNAT2 PAT (i.e., ZDHHC17) activity in axons might stimulate NMNAT2 anterograde transport, potentially increasing NMNAT2 in extreme distal axons, while reducing its levels in more proximal axons. Such disruption of the NMNAT2 gradient could lead to "mixed messages" regarding proximal versus distal axonal health. ZDHHC17's somatic localization circumvents this issue.

Potential Advantages of DLK and NMNAT2 Regulation by a Common PAT

One reason that a single PAT, ZDHHC17, regulates both DLK and NMNAT2 may be that such a system can more readily be ramped up or down by coordinated expression of these three proteins. Indeed, expression of both *Dlk (Map3k12)* and *Nmnat2* correlates better with *Zdhhc17* than with any other PAT (Figures S3E, S3F, S4H, and S4I). *Zddhc21* expression also correlates with that of *Dlk* and *Nmnat2* (Figures S3E, S3F, S4H, and S4I), but *depilated* mice, which lack active ZDHHC21 (Mill et al., 2009), do not phenocopy loss of ZDHHC17, DLK, or NMNAT2. However, we cannot exclude minor roles for ZDHHC21 or other PATs in DLK and/or NMNAT2 regulation.

Why else might ZDHHC17 be the major PAT for DLK and NMNAT2? Intriguingly, ZDHHC17 palmitoylates other axonal/pre-synaptic proteins that undergo vesicular transport (Lemonidis et al., 2015) and may thus localize to a Golgi subdomain via which such palmitoyl proteins transit before budding off into vesicles. Further imaging studies could test this possibility.

Conservation of Palmitoylation-Dependent Control of Axon Integrity and Responses to Damage

ZDHHC17, DLK, and DLK's palmitoyl site are highly conserved (Holland et al., 2016; Roth et al., 2002; Young et al., 2012) and worm ZDHHC17 orthologs control CeDLK-1 localization (Figure 2), which is itself palmitoylation dependent (Holland et al., 2016). ZDHHC17 and DLK are thus likely a conserved enzyme-substrate pair. NMNATs are also evolutionarily ancient. However, NMNAT2's isoform-specific targeting and interaction domain (ISTID) (containing palmitoyl sites BR and zDABM) is vertebrate specific (Lau et al., 2010). Vertebrate NMNAT2s have thus acquired multiple elements that facilitate ZDHHC17-dependent axon survival signals. NMNAT2's localization in neurons and its palmitoylation by ZDHHC17 in non-neuronal cells are both BR/zDABM dependent (Figures 4E, 4F, S4D, and S4E). Determining the extent to which the zDABM that governs palmitoylation of DLK by ZDHHC17 and DLK/ZDHHC17 colocalization in non-neuronal cells (Figures S2D-S2G) also controls DLK/ZDHHC17 localization in mammalian neurons will be an interesting extension of this work. It will likewise be worthwhile to determine whether loss of ZDHHC17 affects not just palmitoylation (Figures 2D-2F, 4C, and 4D) but also localization of DLK and NMNAT2 in mammalian neurons.

Unique Properties of Palmitoylation May Facilitate DLK and NMNAT2 Regulation

Vesicle targeting is critical for axonal trafficking of both DLK and NMNAT2 (Holland et al., 2016; Milde et al., 2013), but why might palmitoylation, rather than a different lipid modification, attach these two proteins to vesicles? Importantly, myristoylation and prenylation modify protein N and C termini, respectively, but palmitoylation can modify the "core" of a protein sequence and can thus more readily regulate protein function (Montersino and Thomas 2015). Indeed, the dual control of DLKinteractions and kinase activity by palmitoylation may minimize phosphorylation of inappropriate substrates (Montersino and Thomas 2015). However, palmitoyl-DLK is also found in uninjured neurons, so palmitoylation is unlikely to be the DLK "on" switch per se (Holland et al., 2016).

Intriguingly, palmitoyl- and ISTID mutant NMNAT2s are more active than WT-NMNAT2 *in vitro* (Lau et al., 2010; Mayer et al., 2010). Thus, although palmitoylation allows NMNAT2 vesicular trafficking, a second unique feature of this modification, its reversibility, may help detach NMNAT2 from vesicles to increase its activity and maximally protect axons. Identifying the axonal thioesterase(s) that depalmitoylates NMNAT2 (and DLK) is a key area for future study.

A Holistic View of the Control of Neuronal Integrity

Knowledge of somal and distal axon degeneration has greatly increased (Coleman and Freeman 2010; Gerdts et al., 2016; Wang et al., 2012; Welsbie et al., 2017). However, many RGC studies have assessed only one of these processes in isolation, and on the few occasions when both were examined, results implicated separate, compartmentalized pathways (Fernandes et al., 2014, 2018). We propose that the control of somal and distal axon integrity might instead be considered as a single, holistic process, involving two palmitoylation-dependent pathways acting in concert, even when physical injury prevents communication between them.

STAR★METHODS

RESOURCE AVAILABILITY

Lead Contact—Further information and requests for resources and reagents should be directed to and will be fulfilled by the Lead Contact, Gareth Thomas (gareth.thomas@temple.edu)

Materials Availability—Plasmids generated in this study are available from the Lead Contact. *C. elegans* strains are deposited to Caenorhabditis Genetics Center (CGC). Requests for *Zdhhc17*$^{f/f}$ mice should be directed to Dr. Michael Hayden (mrh@cmmt.ubc.ca) and may require an MTA.

Data and Code Availability—The published article includes all datasets generated or analyzed during this study.

EXPERIMENTAL MODEL AND SUBJECT DETAILS

Mice—Wild-type C57/B6 and *Zdhhc17*$^{f/f}$ mice (latter on FVB background; Sanders et al., 2016) were housed in a barrier facility in the Lewis Katz School of Medicine at Temple University. The facility utilizes a 12h:12h light:dark cycle, and mice were provided food and water *ad libitum* and were checked daily by ULAR staff. All procedures involving vertebrate animals followed National Institutes of Health guidelines and were approved by the Institutional Animal Care and Use Committee (IACUC) of Temple University.

Rats—Timed-pregnant female Sprague Dawley rats (Strain code 400, Charles River) were euthanized at E16 as previously described (Holland et al., 2016) and embryos of both sexes were used for dissociation of DRG neurons.

Caenorhabditis elegans—The nematode *Caenorhabditis elegans* was also used as an experimental model for this study. All experiments were performed with hermaphrodite animals; males were used only for crosses.

Cell lines—HEK293T cells for biochemical experiments and lentiviral production were obtained from American Type Culture Collection. AAV-pro® 293T Cell Line for AAV production was from Takara Bio. Both cell lines were cultured in DMEM containing 10% (v/v) Fetal Bovine Serum and were routinely checked for mycoplasma contamination and found to be negative.

METHOD DETAILS

AAV Vectors and Preparation—Vector pAAV-hSyn-hChR2(H134R)-eYFP (Addgene plasmid #26973) was modified to replace the hChR2(H134R)-eYFP fragment with shRNA resistant forms of WT-DLK or DLK-CS carrying a C-terminal Hemagglutinin (HA) tag. Generation of shRNA-resistant WT-DLK and DLK-CS was previously described (Holland et al., 2016) and the HA epitope was added by PCR. The same parent plasmid was also cut with *MluI and HindIII* to replace the hSyn-hChR2(H134R)-eYFP fragment with a cassette (synthesized by Genewiz) containing an H1 promoter and DLK shRNA flanked by *PacI* restriction sites (Holland et al., 2016) followed by the human synapsin promoter, an additional PspXI site, Kozak sequence and eGFP cDNA. The resultant vector, termed pAAV-DLKsh-GFP was cut with *PacI* and re-ligated to remove the H1 promoter / DLKshRNA fragment, generating pAAV-GFP. pAAV-GFP was cut with PspXI / HindIII to replace eGFP with a cassette coding for Cre recombinase followed by a self-cleaving T2A sequence and eGFP (synthesized by Genewiz). The resultant vector was termed pAAV-Cre-T2A-GFP. pAAV-GFP was also cut with PspXI / HindIII to replace eGFP with a cassette coding for a cytosolic form of NMNAT1 (Sasaki et al., 2006) with a C-terminal HA-tag (synthesized by Genewiz).

Adeno-associated viruses were made in HEK293T cells by co-transfecting each of the above plasmids with pAAV2 (pACG2)-RC triple mutant (Y444, 500, 730F) (Petrs-Silva et al., 2011) and pHelper (Stratagene, La Jolla, California) plasmids. Cells were lysed 72h post-transfection to release viral particles, which were precipitated using 40% (w/v) polyethylene glycol and purified by cesium chloride density gradient centrifugation. Fractions with refractive index from 1.370 to 1.374 were dialyzed in MWCO 7000 Slide-A-Lyzer cassettes (Thermo Fisher Scientific, Waltham, Massachusetts) overnight at 4°C. AAV titers used for this study were in the range of $1.5–2.5 \times 10^{12}$ genome copies (GC)/ml determined by real-time PCR.

Lentiviral Vectors and Preparation—Lentiviral vectors carrying DLK shRNA or shRNA-resistant DLK rescue constructs were previously described (Holland et al., 2016). cDNAs for mouse Zdhhc3, Zdhhc5, Zdhhc7, Zdhhc10, Zdhhc14, Zdhhc15 (all kind gifts of Masaki Fukata; Fukata et al., 2004) were subcloned from their original vectors into modified FEW vector downstream of an N-terminal HA tag. A previously reported Zdhhc17 cDNA (Fukata et al., 2004) was subcloned into modified FEW vector downstream of a C-terminal HA tag (termed ‘FEW-HA’) with the addition of the N-terminal sequence

atgcagcgggaggagggatttaacaccaag (corresponding amino acid sequence: MQREEGFNTK). This sequence includes the first potential Kozak/start site, as previously reported (Huang et al., 2004; Singaraja et al., 2002). Zdhhc17 N100A mutant (Verardi et al., 2017) was generated by Splicing by Overlap Extension (SOE) PCR using the Zdhhc17 cDNA template and the resultant product was subcloned into FEW-HA. DLK-GFP cDNA was previously described (Holland et al., 2016). The DLK-PVAA-GFP mutant was made by replacing the WT-DLK-GFP XhoI-EcoRI fragment with a similar fragment (synthesized by Genewiz) in which codons coding for Met134 and Ile135 were both mutated to code for Ala. The cDNA of WT rat NMNAT2 was synthesized by Genewiz with XhoI and NotI extensions at the 5′ and 3′ end, respectively and subcloned into FEW-myc and FEW-GFP vectors. NMNAT2-4A mutant was made by replacing the WTNMNAT2 XhoI-BstEII fragment with a similar fragment (synthesized by Genewiz) in which codons coding for Pro124, Val125, Gln128 and Pro129 were all mutated to code for Ala. NMNAT2-3BR mutant was made by replacing the WTNMNAT2 BstEII-NotI fragment with a similar fragment (synthesized by Genewiz) in which codons coding for Lys152, Lys155 and Arg172 were all mutated to code for Ala (‘3BR’ fragment). The NMNAT2 4A-3BR mutant was made by removing the BstEII-NotI fragment of NMNAT2-4A and replacing it with the 3BR fragment described above.

One shRNA against rat Zdhhc17 (sequence 5′-ATGAATGCCAGGAGATACAAGCACTTTAA-3′) was purchased from Origene and subcloned into lentiviral vector FEGW (Holland et al., 2016) together with its neighboring U6 promoter. A cassette containing a second shRNA against rat Zdhhc17 (sequence: 5′-CATTAAAGCTACAGAAGAA-3′ plus a neighboring H1 promoter was gene synthesized (Genewiz) and subcloned into FEGW. ShRNA against rat Zdhhc5 in vector FUGW was previously described (Thomas et al., 2012). ShRNA against rat Zdhhc8 (5′-CAGGATGCCACTCTCAGTGAGCCTAAAGC-3′; Origene) was used in its original vector (Collura et al., 2020). Lentiviral particles from all cDNA- and shRNA-expressing vectors were generated as previously described (Holland et al., 2016).

Intravitreal Injection, Optic Nerve Crush and Whole mount Retina Immunostaining—Intravitreal injection of AAV and subsequent optic nerve crush were conducted as previously described (Miao et al., 2016). Briefly, mice were anesthetized with 0.01 mg xylazine + 0.08 mg ketamine per gram of body weight. For studies of c-Jun phosphorylation and RGC viability involving DLK and its palmitoylation (Figures 1 and S1), 2 μL AAV was injected into the vitreous chamber of 4-week old C57BL/6 mice. Optic nerve crush (ONC) was performed 10 days after AAV injection. Three days (for assessment of c-Jun phosphorylation) or 3 weeks (for assessment of RGC viability) post-ONC, mice were again anesthetized with xylazine/ketamine as above and transcardially perfused with 4% paraformaldehyde (PFA) in PBS. For P-c-Jun studies in *Zdhhc17*$^{f/f}$ mice, 37-day-old mice were anesthetized as above, optic nerve crush was performed 9 days post-injection and mice were reanesthetized and perfused 33 hours post-ONC. The times post-AAV injection (9 days versus 14 days) and times post-ONC (33 h versus 3 days) were shorter for our *Zdhhc17* studies than for our palmitoyl-DLK studies (Figure 1) to minimize potential secondary effects (because we reasoned that ZDHHC17 loss might affect more cellular processes than DLK loss). For caspase-3 studies in *Zdhhc17*$^{f/f}$ mice, 35-day-old mice were anesthetized as

above, optic nerve crush was performed 14 days post-injection and mice were reanesthetized and perfused 6 days post-ONC.

In all *in vivo* experiments, following perfusion with 4% PFA/1 x PBS, eyeballs were subsequently post-fixed for another 2 h prior to dissection of retinas. Whole mount retinal staining was performed silar to a prior report (Miao et al., 2016). Briefly, wide-field images of flat-mounted retinas were acquired using a Nikon 80i epi-fluorescent microscope with a 10x objective (experiments in Figures 1 and S1) or using a Leica SP8 confocal microscope with a 40x oil immersion objective (experiments in Figures 3C-3E, 5D, 5E, and S5).

For studies of optic nerve integrity, mice were anesthetized and intravitreally injected with AAV as above. At 13 or 17 days post-AAV injection, mice were re-anesthetized and transcadially prefused as above. Optic nerves (ONs) were isolated and subjected to post-fixation with 4% PFA at 4°C overnight. ONs were then washed with PBS and incubated in 30% sucrose solution (in PBS) for at least 24 h at 4°C for cryoprotection, and then were embedded in Optimal Cutting Temperature (OCT) medium and frozen on dry ice. Thirty-micron-thick sections were prepared using a cryostat, and collected in PBS. Free-floating ON sections were immunostained with GFP, HA and CD68 antibodies.

Lentiviral Infection, Trophic Deprivation and Imaging of DRG Neuron cultures —Dorsal root ganglion (DRG) neurons were dissociated from E16 rat embryos and conventional ‘mass’ cultures were prepared as previously described (Holland et al., 2016). For TD experiments and Acyl Biotin Exchange assays (ABE – see detailed description below), neurons were infected with lentivirus at two days *in vitro* (DIV2) and subjected to Trophic Deprivation (TD) at DIV6 or DIV8 (latter time point used for *Zdhhc17* shRNA experiments to ensure complete *Zdhhc17* knockdown). For all TD experiments, NGF-containing medium was replaced with fresh Neurobasal medium lacking NGF but containing B27 supplement plus 25 μg/mL sheep anti-NGF antibody. Neurons were subsequently lysed or fixed at the time points indicated in individual Figures. For studies of NMNAT2 distribution (Figure 4), neurons were infected with lentivirus at DIV6 and fixed at DIV8. For studies of HA-ZDHHC17 distribution (Figure 4), neurons were virally infected at DIV4 and imaged at DIV10. For studies of endogenous ZDHHC17 distribution, microfluidic cultures were prepared as previously described (Holland et al., 2016) and the ‘soma + axons’ and ‘distal axons’ chambers were lysed by addition of SDS sample buffer. The ‘Axons’ chamber was lysed in 1/12 of the volume used for the ‘Soma + Axons’ chamber to account for the lower amount of material in the former compartment.

For studies of long-term axonal viability (Figure 5), DRG neurons were lentivirally infected on DIV2. In some experiments, sister cultures were infected with AAV expressing HA-cytoNMNAT1 on DIV1. In some experiments, 1mM NAD^+ was added on alternate days after lentiviral infection. In all cases, bright field images were acquired on DIV11-12.

For immunocytochemical readouts, dissociated DRG neurons cultured on coverslips were rinsed once with 1x Recording buffer (25mM HEPES pH7.4, 120mM NaCl, 5mM KCl, 2mM $CaCl_2$, 1mM $MgCl_2$, 30mM Glucose) and fixed in 4% paraformaldehyde (PFA)/ sucrose for 10 min at room temperature. Samples were permeabilized in PBS containing

0.25% (w/v) Triton X-100 for 10 min at 4°C, blocked with PBS containing 10% (v/v) Normal Goat Serum (SouthernBiotech, 0060-01) for 1 h and incubated in primary antibodies overnight at 4°C in blocking solution. After 3 washes with PBS, cells were incubated for 1 h at room temperature with AlexaDye-conjugated fluorescent secondary antibodies diluted in blocking solution, prior to 3 final PBS washes and mounting in FluorSave reagent (Millipore Sigma).

Image Analysis of Retinas and Optic Nerves—To quantify c-Jun phosphorylation in AAV-infected retinas for experiments involving DLK knockdown and rescue, images of GFP and P-c-Jun fluorescent signals were thresholded in Fiji (Schindelin et al., 2012) and GFP/P-c-Jun double-positive cells per field were counted. To quantify surviving RGCs in Figure 1, images of GFP and RBPMS fluorescent signals were thresholded in Fiji and GFP/RBPMS double positive cells per field were counted. To quantify c-Jun phosphorylation in AAV-infected retinas for experiments involving *Zdhhc17* CKO, images were thresholded as above and GFP-positive RGCs were scored as P-c-Jun-positive or –negative by an experimenter blinded to genotype. In each case, 3-4 images were acquired per individual retina and the number of cells per image was averaged to generate a single determination.

Degeneration of optic nerve axons was quantified using optic nerve confocal images from mice that had been intravitreally injected with AAV to express GFP plus/minus Cre. The 5 consecutive most intensely GFP-positive slices for each mouse were marked and each of the five images was then thresholded to an identical value across conditions. Infected (GFP-positive) axonal fragments (‘blebs’) were quantified by analyzing particles of defined size (size: 10-infinity pixels, circularity: 0.40-1.00) in ImageJ for each of the 5 z-slice images per individual sample. The number of axon blebs per field was then averaged to generate a single determination. To quantify microgliosis, CD68 signal was analayzed in the same z-slice images. Each image was again thresholded to an identical value and CD68-positive signal was detected by analyzing particles (size: 5-infinity, circularity: 0.0-1.0) in ImageJ. The CD68-positive area was then plotted as a percentage of the total area of the field imaged.

To quantify surviving RGCs in Figure S5, images of RBPMS immunofluorescence were counted manually, guided by overlapping DAPI signal to identify RGC nuclei.

Image Analysis in Cultured Neurons—c-Jun phosphorylation in cultured DRG neurons was quantified using ImageJ’s cell batch count plugin. Images were thresholded for P-c-Jun and NeuN signal and the percentage of P-c-Jun positive cells that were also NeuN-positive was calculated. To quantify NMNAT2 axonal distribution, maximum intensity projections of confocal images of NMNAT2-WT-myc or NMNAT2-4A-3BR-myc were thresholded to an identical value in ImageJ. Tuj1 signal from the same images was separately thresholded (to a different absolute value, but again identically across conditions). Regions of the myc and Tuj1 images that contained cell somas were manually identified and cropped. The thresholded Tuj1 signal was used as a mask and the number of NMNAT2-myc puncta that overlapped with the Tuj1 mask was counted by analyzing particles (size: 6-30 pixels, circularity: 0.6-1.0) in ImageJ.

To assess HA-ZDHHC17 distribution, maximum intensity projections of confocal images of HA-, GM130 (Golgi marker) and coinfected GFP immunostaining were generated. Line intensity profile plots from HA and GM130 (Golgi marker) channels were overlaid in ImageJ.

To quantify axon degeneration, images of distal axons were acquired live and subsequently ranked on a 5-point scale (0 = no degeneration to 5 = severe degeneration), according to the degree of observed axon fragmentation and beading, similar to a prior report (Yang et al., 2015).

Detection of Palmitoylation by Acyl Biotinyl Exchange (ABE) assay—ABE assays and subsequent western blotting were performed similar to a prior report (Holland et al., 2016). Briefly, transfected HEK293T cells or neurons were lysed in 50 mM HEPES pH 7.0, 2% (w/v) SDS, 1 mM EDTA plus protease inhibitor mixture (PIC, Roche), and 20 mM methyl-methane thiosulfonate (MMTS, to block free thiols). Unreacted MMTS was removed by acetone precipitation and pellets were resuspended in buffer containing 4% (w/v) SDS. Samples were diluted and incubated at room temperature for 1 h in the presence of sulfhydryl-reactive (HPDP-) biotin plus either 0.7M hydroxylamine pH 7.4 (to cleave thioester bonds) or 50 mM Tris pH 7.4. Hydroxylamine/Tris and unreacted HPDP-biotin were removed by acetone precipitation and pellets were resuspended in lysis buffer without MMTS. SDS was diluted to 0.1% (w/v) and biotinylated (i.e., previously palmitoylated) proteins in the samples were affinity-purified using neutravidin-conjugated beads. Beta-mercaptoethanol [1% (v/v)] was used to cleave HPDP-biotin and release purified proteins from the beads. The released proteins in the supernatant were denatured in SDS sample buffer and processed for SDS/PAGE and subsequent western blotting. For all quantified data, western blot signals for a given palmitoyl-protein in ABE fractions were normalized to total levels of the same protein in parent lysates.

HEK293T Cell ABE and Co-immunoprecipitation Experiments—HEK293T cells were transfected using a calcium phosphate based method as described (Holland et al., 2016). Processing of lysates for ABE assays or for co-immunoprecipitations was also performed similar to Holland et al. (2016). For the latter experiments, HEK293T cells were transfected with C-terminally GFP-tagged DLK cDNA plus the indicated HA-tagged ZDHHC cDNAs or empty vector. All ZDHHC cDNAs were N-terminally tagged except for ZDHHC17, which was C-terminally tagged. The following day cells were lysed with ice-cold Immunoprecipitation buffer (IPB; 20 mM Tris pH 7.5, 150 mM NaCl 0.1% Triton X-100 plus protease and phosphatase inhibitors). Lysates were incubated at 4°C for 30 min while rotating prior to centrifugation at 13,000 x *g* and passage through a SpinX column to remove debris. After centrifugation of lysates, a fraction of each supernatant was diluted in sample buffer, denatured, and run on PAGE gels as ‘inputs.’ Remaining supernatants were immunoprecipitated for 90 min at 4°C with anti-HA antibodies that had been precoupled to protein G Sepharose beads (GE Healthcare). Beads were washed three times with ice cold IPB containing 0.25M NaCl and twice with IPB. Proteins were eluted with SDS sample buffer and subjected to SDS-PAGE and subsequent immunoblotting.

HEK293T Cell Immunocytochemical Experiments—Distribution of DLK-GFP in HEK293T cells was assessed by fixing and permeabilizing cells on coverslips 8 h after calcium phosphate-based transfection. Incubation with primary and secondary antibodies was performed as described for cultured neurons.

Bio-infomatic Analyses—To identify palmitoyl-motifs similar to that of DLK, the sequence surrounding DLK's palmitoyl-site FGCLRP (where C is the palmitoylated Cys-127) was broadened to account for possible amino acid conservation to give the modified sequence [FIL][GAC]C[VIL][RK] P. This modified sequence was entered in the 'Search using Regular Expressions' tool of Scansite 4.0 (Obenauer et al., 2003) to identify instances of this motif present in UniProt/SwissProt that are conserved in mouse, rat and human orthologs of a given protein. Only three proteins matching these criteria were identified; DLK (MAP3K12), NMNAT2 and Importin alpha-5. A search of the online Swisspalm database (Blanc et al., 2015) revealed that only DLK and NMNAT2, but not Importin alpha-5, have been previously identified as palmitoyl-proteins, supporting the conclusion that the palmitoyl-motifs of DLK and NMNAT2 are more similar to one another than to any other known palmitoyl-site.

To assess co-expression of DLK and NMNAT2 with ZDHHC-PATs, expression of DLK(*Map3k12*), *Nmnat2* and all 23 mouse *Zdhhc*-PATs from 265 identified nervous system cell subtypes was extracted from mousebrain.org (an online resource containing single cell RNA-Seq data from Zeisel et al., 2018 and related studies). *Map3k12* expression values in each of the 265 cell types were then plotted in GraphPad Prism against expression values for each PAT individually, generating 23 separate scatterplots. The r-squared value for correlation of each PAT's expression versus that of *Map3k12* was then calculated in GraphPad Prism and logged. The same analysis was repeated to compare *Nmnat2* expression values versus expression values for each PAT

C. elegans* genetics—C. elegans* strains were maintained at 20°C on NGM plates as described (Brenner 1974). Plasmid Pmec-4-GFP::CeDLK-1L(WT)-3′UTR(let-858) (pCZGY2335) was previously described (Holland et al., 2016). The integrated line *juIs501* was generated in CZ20310 *Pmex-5-His-72::miniSOG(juSi164) unc-119(ed3) III* background, following the protocol described in Noma and Jin (2018). *juIs501* was then outcrossed to wild-type N2 several times to remove *juSi164* and *unc-119*. Strains were constructed following standard mating procedure, and are listed in STAR Methods table. Sequences of primers used to genotype individual alleles are listed in Table S1.

CRISPR/Cas9 Knock-out of *dhhc-13*—*dhhc-13(ju1673)* was generated following a protocol described in Arribere et al. (2014). Briefly, sgRNAs targeting exon 1 and exon 11 of *dhhc-13* were synthesized as CRISPR-Cas9 crRNA (IDT Alt-R®). The microinjection mixture contained *dhhc-13* crRNAs (10 μM), *dpy-10* crRNA (5 μM), tracrRNA (15 μM) and Cas9 protein (28 μM). F1 progeny with dumpy bodies were selected for propagation and their progeny in turn were screened for deletions in *dhhc-13* by PCR using 3 primers (YJ12385, YJ12386, YJ12387). *dhhc-13(ju1673)* was a 3.7kb deletion, removing the majority of protein-coding region, hence a null allele.

Fluorescence Microscopy in *C. elegans*—To quantify the subcellular localization of *C. elegans* DLK-1 in PLM touch receptor neuron using *juIs501[Pmec-4-GFP::DLK-1L, Pmec-4-tagRFP]*, L4 animals were mounted in M9 buffer on a 10% agarose pad. GFP-DLK-1L pattern in PLM was scored under a Zeiss Axioplan 2 microscope equipped with Chroma HQ filters and a 63x objective. Punctate GFP-DLK-1 was scored as visibly detectable GFP puncta in both soma or axon of PLM . Diffuse GFP-DLK-1 generally showed decreased fluorescence intensity in axon and soma. All strains were quantified in a genotype-blind manner and data were collected from a minimum of 3 independent observations (30-70 animals per observation) on different days. Representative fluorescent images of PLM neurons in Figure 2D were acquired from day 1 adults using a Zeiss LSM710 confocal microscope equipped with a 63x objective. Images are maximal intensity projections from z stacks (0.5-1 μm/section).

QUANTIFICATION AND STATISTICAL ANALYSIS

All data were analyzed using GraphPad Prism software (GraphPad Software, San Diego, CA). In all graphs the mean is shown and error bars indicate standard error of the mean (SEM). Statistical tests used and values of p and N are indicated in the corresponding figure legend. For mammalian *in vivo* experiments, N refers to the number of animals per condition. For experiments involving cultured mammalian cells, N refers to the number of individual wells or plates per condition. All experiments using cultured cells were repeated from at least two different dissections or platings.

Supplementary Material

Refer to Web version on PubMed Central for supplementary material.

ACKNOWLEDGMENT

We thank Drs. F. Qin and Y. Liu for AAVs, Dr. C. Su (UCSD) for invaluable discussions, Dr. K. Noma for generating *juIs501*, and Dr. M. Fukata for *Zdhhc* cDNAs. This work was supported by NIH (R01NS094402 and R21EY029386 [G.M.T.], R37NS035546 [Y.J.], and R01EY024932, R01EY023295, and R01EY028106 [Y.H.]), Shriners Hospitals for Children (no. 85600 and no. 85190 PHI [G.M.T.] and a Special Shared Facility Grant to the Shriners Neural Repair Viral Core [G.M.S.]), and BrightFocus Foundation (G2019267 [G.T.]). S.S.S. acknowledges a Brody Family Medical Trust Fund Fellowship.

REFERENCES

Argyriou AA, Kyritsis AP, Makatsoris T, and Kalofonos HP (2014). Chemotherapy-induced peripheral neuropathy in adults: a comprehensive update of the literature. Cancer Manag. Res 6, 135–147. [PubMed: 24672257]

Arribere JA, Bell RT, Fu BX, Artiles KL, Hartman PS, and Fire AZ (2014). Efficient marker-free recovery of custom genetic modifications with CRISPR/Cas9 in Caenorhabditis elegans. Genetics 198, 837–846. [PubMed: 25161212]

Beirowski B, Babetto E, Coleman MP, and Martin KR (2008). The WldS gene delays axonal but not somatic degeneration in a rat glaucoma model. Eur. J. Neurosci 28, 1166–1179. [PubMed: 18783366]

Berger F, Lau C, Dahlmann M, and Ziegler M (2005). Subcellular compartmentation and differential catalytic properties of the three human nicotinamide mononucleotide adenylyltransferase isoforms. J. Biol. Chem 280, 36334–36341. [PubMed: 16118205]

Blanc M, David F,Abrami L, Migliozzi D, Armand F, Bürgi J, and van der Goot FG (2015). SwissPalm: Protein Palmitoylation database. F1000Res. 4, 261. [PubMed: 26339475]

Brenner S (1974). The genetics of Caenorhabditis elegans. Genetics 77, 71–94. [PubMed: 4366476]

Coleman MP, and Freeman MR (2010). Wallerian degeneration, wld(s), and nmnat. Annu. Rev. Neurosci 33, 245–267. [PubMed: 20345246]

Collura KM, Niu J, Sanders SS, Montersino A, Holland SM, and Thomas GM (2020). The palmitoyl acyltransferases ZDHHC5 and ZDHHC8 are uniquely present in DRG axons and control retrograde signaling via the Gp130/JAK/STAT3 pathway. Journal of Biological Chemistryjbc.RA120.013815, In press. 10.1074/jbc.RA120.013815.

Deshmukh M, Kuida K, and Johnson EM Jr. (2000). Caspase inhibition extends the commitment to neuronal death beyond cytochrome c release to the point of mitochondrial depolarization. J. Cell Biol 150, 131–143. [PubMed: 10893262]

Dragatsis I, Levine MS, and Zeitlin S (2000). Inactivation of Hdh in the brain and testis results in progressive neurodegeneration and sterility in mice. Nat. Genet 26, 300–306. [PubMed: 11062468]

Ebneter A, Casson RJ, Wood JP, and Chidlow G (2010). Microglial activation in the visual pathway in experimental glaucoma: spatiotemporal characterization and correlation with axonal injury. Invest. Ophthalmol. Vis. Sci 51, 6448–6460. [PubMed: 20688732]

Edmonds MJ, and Morgan A (2014).A systematic analysis of protein palmitoylation in Caenorhabditis elegans. BMC Genomics 15, 841. [PubMed: 25277130]

Ernst AM, Syed SA, Zaki O, Bottanelli F, Zheng H, Hacke M, Xi Z, Rivera-Molina F, Graham M, Rebane AA, et al. (2018). S-palmitoylation sorts membrane cargo for anterograde transport in the Golgi. Dev. Cell 47, 479–493.e7. [PubMed: 30458139]

Fernandes KA, Harder JM, Fornarola LB, Freeman RS, Clark AF, Pang IH, John SW, and Libby RT (2012). JNK2 and JNK3 are major regulators of axonal injury-induced retinal ganglion cell death. Neurobiol. Dis 46, 393–401. [PubMed: 22353563]

Fernandes KA, Harder JM, John SW, Shrager P, and Libby RT (2014). DLK-dependent signaling is important for somal but not axonal degeneration of retinal ganglion cells following axonal injury. Neurobiol. Dis 69, 108–116. [PubMed: 24878510]

Fernandes KA, Mitchell KL, Patel A, Marola OJ, Shrager P, Zack DJ, Libby RT, and Welsbie DS (2018). Role of SARM1 and DR6 in retinal ganglion cell axonal and somal degeneration following axonal injury. Exp. Eye Res 171, 54–61. [PubMed: 29526794]

Fernández-Chacón R, Wölfel M, Nishimune H, Tabares L, Schmitz F, Castellano-Muñoz M, Rosenmund C, Montesinos ML, Sanes JR, Schneggenburger R, and Südhof TC (2004). The synaptic vesicle protein CSP alpha prevents presynaptic degeneration. Neuron 42, 237–251. [PubMed: 15091340]

Fukata M, Fukata Y, Adesnik H, Nicoll RA, and Bredt DS (2004). Identification of PSD-95 palmitoylating enzymes. Neuron 44, 987–996. [PubMed: 15603741]

Gerdts J, Summers DW, Milbrandt J, and DiAntonio A (2016). Axon self-destruction: new links among SARM1, MAPKs, and NAD+ metabolism. Neuron 89, 449–460. [PubMed: 26844829]

Ghosh AS, Wang B, Pozniak CD, Chen M, Watts RJ, and Lewcock JW (2011). DLK induces developmental neuronal degeneration via selective regulation of proapoptotic JNK activity. J. Cell Biol 194, 751–764. [PubMed: 21893599]

Gilley J, and Coleman MP (2010). Endogenous Nmnat2 is an essential survival factor for maintenance of healthy axons. PLoS Biol. 8, e1000300. [PubMed: 20126265]

Gilley J, Orsomando G, Nascimento-Ferreira I, and Coleman MP (2015). Absence of SARM1 rescues development and survival of NMNAT2-deficient axons. Cell Rep. 10, 1974–1981. [PubMed: 25818290]

Gilley J, Ribchester RR, and Coleman MP (2017). Sarm1 deletion, but not Wld^S, confers lifelong rescue in a mouse model of severe axonopathy. Cell Rep. 21, 10–16. [PubMed: 28978465]

Greaves J, Gorleku OA, Salaun C, and Chamberlain LH (2010). Palmitoylation of the SNAP25 protein family: specificityand regulation by DHHC palmitoyl transferases. J. Biol. Chem 285, 24629–24638. [PubMed: 20519516]

Holland SM, Collura KM, Ketschek A, Noma K, Ferguson TA, Jin Y, Gallo G, and Thomas GM (2016). Palmitoylation controls DLK localization, interactions and activity to ensure effective axonal injury signaling. Proc. Natl. Acad. Sci. USA 113, 763–768. [PubMed: 26719418]

Howell GR, Soto I, Libby RT, and John SW (2013). Intrinsic axonal degeneration pathways are critical for glaucomatous damage. Exp. Neurol 246, 54–61. [PubMed: 22285251]

Huang K, Yanai A, Kang R, Arstikaitis P, Singaraja RR, Metzler M, Mullard A, Haigh B, Gauthier-Campbell C, Gutekunst CA, et al. (2004). Huntingtin-interacting protein HIP14 is a palmitoyl transferase involved in palmitoylation and trafficking of multiple neuronal proteins. Neuron 44, 977–986. [PubMed: 15603740]

Huang K, Sanders SS, Kang R, Carroll JB, Sutton L, Wan J, Singaraja R, Young FB, Liu L, El-Husseini A, et al. (2011). Wild-type HTT modulates the enzymatic activity ofthe neuronal palmitoyl transferase HIP14. Hum. Mol. Genet 20, 3356–3365. [PubMed: 21636527]

Kwong JM, Quan A, Kyung H, Piri N, and Caprioli J (2011). Quantitative analysis of retinal ganglion cell survival with Rbpms immunolabeling in animal models of optic neuropathies. Invest. Ophthalmol. Vis. Sci 52, 9694–9702. [PubMed: 22110060]

Lau C, Dölle C, Gossmann TI, Agledal L, Niere M, and Ziegler M (2010). Isoform-specific targeting and interaction domains in human nicotinamide mononucleotide adenylyltransferases. J. Biol. Chem 285, 18868–18876. [PubMed: 20388704]

Lemonidis K, Sanchez-Perez MC, and Chamberlain LH (2015). Identification of a novel sequence motif recognized by the ankyrin repeat domain of zDHHC17/13 S-acyltransferases. J. Biol. Chem 290, 21939–21950. [PubMed: 26198635]

Lemonidis K, MacLeod R, Baillie GS, and Chamberlain LH (2017). Peptide array-based screening reveals a large number of proteins interacting with the ankyrin-repeat domain of the zDHHC17 S-acyltransferase. J. Biol. Chem 292, 17190–17202. [PubMed: 28882895]

Li Y, Schlamp CL, and Nickells RW (1999). Experimental induction of retinal ganglion cell death in adult mice. Invest. Ophthalmol. Vis. Sci 40, 1004–1008. [PubMed: 10102300]

Li Y, Schlamp CL, Poulsen KP, and Nickells RW (2000). Bax-dependent and independent pathways of retinal ganglion cell death induced by different damaging stimuli. Exp. Eye Res 71, 209–213. [PubMed: 10930325]

Libby RT, Li Y, Savinova OV, Barter J, Smith RS, Nickells RW, and John SW (2005). Susceptibility to neurodegeneration in a glaucoma is modified by Bax gene dosage. PLoS Genet. 1, 17–26. [PubMed: 16103918]

Lois C, Hong EJ, Pease S, Brown EJ, and Baltimore D (2002). Germline Transmission and Tissue-Specific Expression of Transgenes Delivered by Lentiviral Vectors. Science 295, 868–872. [PubMed: 11786607]

Lorber B, Tassoni A, Bull ND, Moschos MM, and Martin KR (2012). Retinal ganglion cell survival and axon regeneration in WldS transgenic rats after optic nerve crush and lens injury. BMC Neurosci. 13, 56. [PubMed: 22672534]

Maes ME, Schlamp CL, and Nickells RW (2017). BAX to basics: how the BCL2 gene family controls the death of retinal ganglion cells. Prog. Retin. Eye Res 57, 1–25. [PubMed: 28064040]

Martin KR, Klein RL, and Quigley HA (2002). Gene delivery to the eye using adeno-associated viral vectors. Methods 28, 267–275. [PubMed: 12413426]

Martin DDO, Kanuparthi PS, Holland SM, Sanders SS, Jeong HK, Einarson MB, Jacobson MA, and Thomas GM (2019). Identification of novel inhibitors of DLK palmitoylation and signaling by high content screening. Sci. Rep 9, 3632. [PubMed: 30842471]

Mayer PR, Huang N, Dewey CM, Dries DR, Zhang H, and Yu G (2010). Expression, localization, and biochemical characterization of nicotinamide mononucleotide adenylyltransferase 2. J. Biol. Chem 285, 40387–40396. [PubMed: 20943658]

Miao L, Yang L, Huang H, Liang F, Ling C, and Hu Y (2016). mTORC1 is necessary but mTORC2 and GSK3β are inhibitory for AKT3-induced axon regeneration in the central nervous system. eLife 5, e14908. [PubMed: 27026523]

Milde S, and Coleman MP (2014). Identification of palmitoyltransferase and thioesterase enzymes that control the subcellular localization of axon survival factor nicotinamide mononucleotide adenylyltransferase 2 (NMNAT2). J. Biol. Chem 289, 32858–32870. [PubMed: 25271157]

Milde S, Gilley J, and Coleman MP (2013). Subcellular localization determines the stability and axon protective capacity of axon survival factor Nmnat2. PLoS Biol. 11, e1001539. [PubMed: 23610559]

Mill P, Lee AW, Fukata Y, Tsutsumi R, Fukata M, Keighren M, Porter RM, McKie L, Smyth I, and Jackson IJ (2009). Palmitoylation regulates epidermal homeostasis and hair follicle differentiation. PLoS Genet. 5, e1000748. [PubMed: 19956733]

Montersino A, and Thomas GM (2015). Slippery signaling: palmitoylation-dependent control of neuronal kinase localization and activity. Mol. Membr. Biol 32, 179–188. [PubMed: 27241460]

Noma K, and Jin Y (2018). Rapid integration of multi-copy transgenes using optogenetic mutagenesis in *Caenorhabditis elegans*. G3 (Bethesda) 8, 2091–2097. [PubMed: 29691291]

Obenauer JC, Cantley LC, and Yaffe MB (2003). Scansite 2.0: proteome-wide prediction of cell signaling interactions using short sequence motifs. Nucleic Acids Res. 31, 3635–3641. [PubMed: 12824383]

Ohno Y, Kihara A, Sano T, and Igarashi Y (2006). Intracellular localization and tissue-specific distribution of human and yeast DHHC cysteine-rich domain-containing proteins. Biochim. Biophys. Acta 1761, 474–483. [PubMed: 16647879]

Palin K, Cunningham C, Forse P, Perry VH, and Platt N (2008). Systemic inflammation switches the inflammatory cytokine profile in CNS Wallerian degeneration. Neurobiol. Dis 30, 19–29. [PubMed: 18255301]

Perry VH (1981). Evidence for an amacrine cell system in the ganglion cell layer of the rat retina. Neuroscience 6, 931–944. [PubMed: 6165929]

Petrs-Silva H, Dinculescu A, Li Q, Deng WT, Pang JJ, Min SH, Chiodo V, Neeley AW, Govindasamy L, Bennett A, et al. (2011). Novel properties of tyrosine-mutant AAV2 vectors in the mouse retina. Mol. Ther 19, 293–301. [PubMed: 21045809]

Roth AF, Feng Y, Chen L, and Davis NG (2002). The yeast DHHC cysteine-rich domain protein Akr1p is a palmitoyl transferase. J. Cell Biol 159, 23–28. [PubMed: 12370247]

Sajgo S, Ghinia MG, Brooks M, Kretschmer F, Chuang K, Hiriyanna S, Wu Z, Popescu O, and Badea TC (2017). Molecular codes for cell type specification in Brn3 retinal ganglion cells. Proc. Natl. Acad. Sci. USA 114, E3974–E3983. [PubMed: 28465430]

Sánchez-Migallón MC, Valiente-Soriano FJ, Nadal-Nicolás FM, Vidal-Sanz M, and Agudo-Barriuso M (2016). Apoptotic retinal ganglion cell death after optic nerve transection or crush in mice: delayed RGC loss with BDNF or a caspase 3 inhibitor. Invest. Ophthalmol. Vis. Sci 57, 81–93. [PubMed: 26780312]

Sanders SS, Parsons MP, Mui KK, Southwell AL, Franciosi S, Cheung D, Waltl S, Raymond LA, and Hayden MR (2016). Sudden death due to paralysis and synaptic and behavioral deficits when Hip14/Zdhhc17 is deleted in adult mice. BMC Biol. 14, 108. [PubMed: 27927242]

Sasaki Y, Araki T, and Milbrandt J (2006). Stimulation of nicotinamide adenine dinucleotide biosynthetic pathways delays axonal degeneration after axotomy. J. Neurosci 26, 8484–8491. [PubMed: 16914673]

Schindelin J,Arganda-Carreras I, Frise E, Kaynig V, Longair M, Pietzsch T, Preibisch S, Rueden C, Saalfeld S, Schmid B, et al. (2012). Fiji: an open-source platform for biological-image analysis. Nat. Methods 9, 676–682. [PubMed: 22743772]

Simon DJ, Pitts J, Hertz NT, Yang J, Yamagishi Y, Olsen O, Tešić Mark M, Molina H, and Tessier-Lavigne M (2016). Axon degeneration gated by retrograde activation of somatic pro-apoptotic signaling. Cell 164, 1031–1045. [PubMed: 26898330]

Singaraja RR, Hadano S, Metzler M, Givan S, Wellington CL,Warby S, Yanai A, Gutekunst CA, Leavitt BR, Yi H, et al. (2002). HIP14, a novel ankyrin domain-containing protein, links huntingtin to intracellular trafficking and endocytosis. Hum. Mol. Genet 11, 2815–2828. [PubMed: 12393793]

Singaraja RR, Huang K, Sanders SS, Milnerwood AJ, Hines R, Lerch JP, Franciosi S, Drisdel RC, Vaid K, Young FB, et al. (2011). Altered palmitoylation and neuropathological deficits in mice lacking HIP14. Hum. Mol. Genet 20, 3899–3909. [PubMed: 21775500]

Thomas GM, Hayashi T, Chiu SL, Chen CM, and Huganir RL (2012). Palmitoylation by DHHC5/8 targets GRIP1 to dendritic endosomes to regulate AMPA-R trafficking. Neuron 73, 482–496. [PubMed: 22325201]

Tran NM, Shekhar K,Whitney IE, Jacobi A, Benhar I, Hong G, Yan W, Adiconis X, Arnold ME, Lee JM, et al. (2019). Single-cell profiles of retinal ganglion cells differing in resilience to injury reveal neuroprotective genes. Neuron 104, 1039–1055.e12. [PubMed: 31784286]

Verardi R, Kim J-S, Ghirlando R, and Banerjee A (2017). Structural basis for substrate recognition by the ankyrin repeat domain of human DHHC17 palmitoyltransferase. Structure 25, 1337–1347.e6. [PubMed: 28757145]

Wang JT, Medress ZA, and Barres BA (2012). Axon degeneration: molecular mechanisms of a self-destruction pathway. J. Cell Biol 196, 7–18. [PubMed: 22232700]

Wang JT, Medress ZA, Vargas ME, and Barres BA (2015). Local axonal protection by WldS as revealed by conditional regulation of protein stability. Proc. Natl. Acad. Sci. USA 112, 10093–10100. [PubMed: 26209654]

Wang G, Liu X, Gaertig MA, Li S, and Li XJ (2016). Ablation of huntingtin in adult neurons is nondeleterious but its depletion in young mice causes acute pancreatitis. Proc. Natl. Acad. Sci. USA 113, 3359–3364. [PubMed: 26951659]

Washbourne P, Thompson PM, Carta M, Costa ET, Mathews JR, Lopez-Benditó G, Molnár Z, Becher MW, Valenzuela CF, Partridge LD, and Wilson MC (2002). Genetic ablation of the t-SNARE SNAP-25 distinguishes mechanisms of neuroexocytosis. Nat. Neurosci 5, 19–26. [PubMed: 11753414]

Watkins TA, Wang B, Huntwork-Rodriguez S, Yang J, Jiang Z, East-ham-Anderson J, Modrusan Z, Kaminker JS, Tessier-Lavigne M, and Lewcock JW (2013). DLK initiates a transcriptional program that couples apoptotic and regenerative responses to axonal injury. Proc. Natl. Acad. Sci. USA 110, 4039–4044. [PubMed: 23431164]

Welsbie DS, Yang Z, Ge Y, Mitchell KL, Zhou X, Martin SE, Berlinicke CA, Hackler L Jr., Fuller J, Fu J, et al. (2013). Functional genomic screening identifies dual leucine zipper kinase as a key mediator of retinal ganglion cell death. Proc. Natl. Acad. Sci. USA 110, 4045–4050. [PubMed: 23431148]

Welsbie DS, Mitchell KL, Jaskula-Ranga V, Sluch VM, Yang Z, Kim J, Buehler E, Patel A, Martin SE, Zhang P-W, et al. (2017). Enhanced functional genomic screening identifies novel mediators of dual leucine zipper kinase-dependent injury signaling in neurons. Neuron 94, 1142–1154.e6. [PubMed: 28641113]

Yamagishi Y, and Tessier-Lavigne M (2016). An atypical SCF-like ubiquitin ligase complex promotes Wallerian degeneration through regulation of axonal Nmnat2. Cell Rep. 17, 774–782. [PubMed: 27732853]

Yang J, Wu Z, Renier N, Simon DJ, Uryu K, Park DS, Greer PA, Tournier C, Davis RJ, and Tessier-Lavigne M (2015). Pathological axonal death through a MAPK cascade that triggers a local energy deficit. Cell 160, 161–176. [PubMed: 25594179]

Young FB, Butland SL, Sanders SS, Sutton LM, and Hayden MR (2012). Putting proteins in their place: palmitoylation in Huntington disease and other neuropsychiatric diseases. Prog. Neurobiol 97, 220–238. [PubMed: 22155432]

Zeisel A, Hochgerner H, Lönnerberg P, Johnsson A, Memic F, van der Zwan J, Häring M, Braun E, Borm LE, La Manno G, et al. (2018). Molecular architecture of the mouse nervous system. Cell 174, 999–1014.e22. [PubMed: 30096314]

Highlights

- The same enzyme, ZDHHC17, palmitoylates DLK and NMNAT2
- DLK palmitoylation by ZDHHC17 is essential for somal responses to axonal injury
- Prolonged loss of ZDHHC17 causes NMNAT-dependent fragmentation of distal axons
- Conserved motifs in NMNAT2 and DLK govern their ZDHHC17-dependent regulation

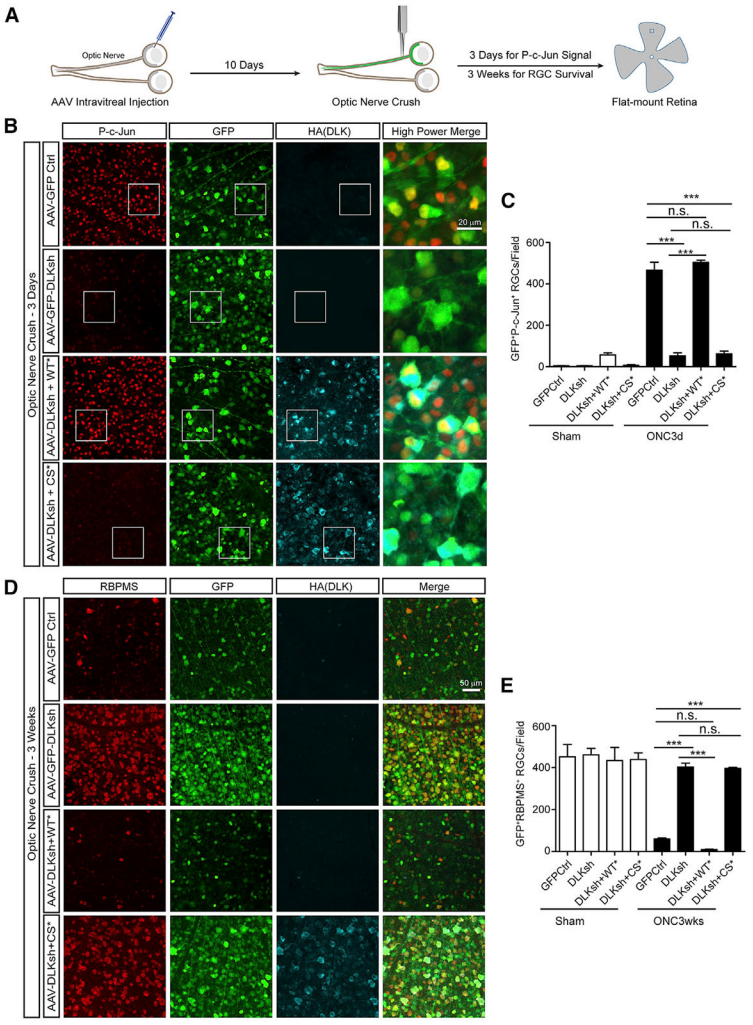

Figure 1. Palmitoyl-DLK Is Essential for Somal Responses to ONC

(A) Experimental setup: blue square shows approximate retinal region used for imaging.

(B) Immunostained retinal flat mounts from eyes injected with the indicated AAVs, fixed 3 days post-ONC. ONC-induced P-c-Jun signal is markedly attenuated by DLKsh-expressing AAV (AAV-GFP-DLKsh) and "rescued" by shRNA-resistant (shr) wild-type DLK (AAV-DLKsh + WT-DLK*-HA ["WT*"]), but not shr-palmitoyl mutant DLK (AAV-DLKsh + DLKCS*-HA ["CS*"]). 4th column, overlay of boxed areas in columns 1–3.

(C) Quantified data from (B) (n = 3–5 per condition); ***p < 0.001; n.s., non-significant. One-way ANOVA; Bonferroni post hoc test.

(D) Immunostained retinal flat mounts from eyes injected with the indicated AAVs, fixed 3 weeks post-ONC. 4th column, overlay of columns 1–3.

(E) Quantified data from (D) (n = 3–5 per condition). ***p < 0.001. One-way ANOVA; Bonferroni post hoc test.

Data in all figures are mean ± SEM.

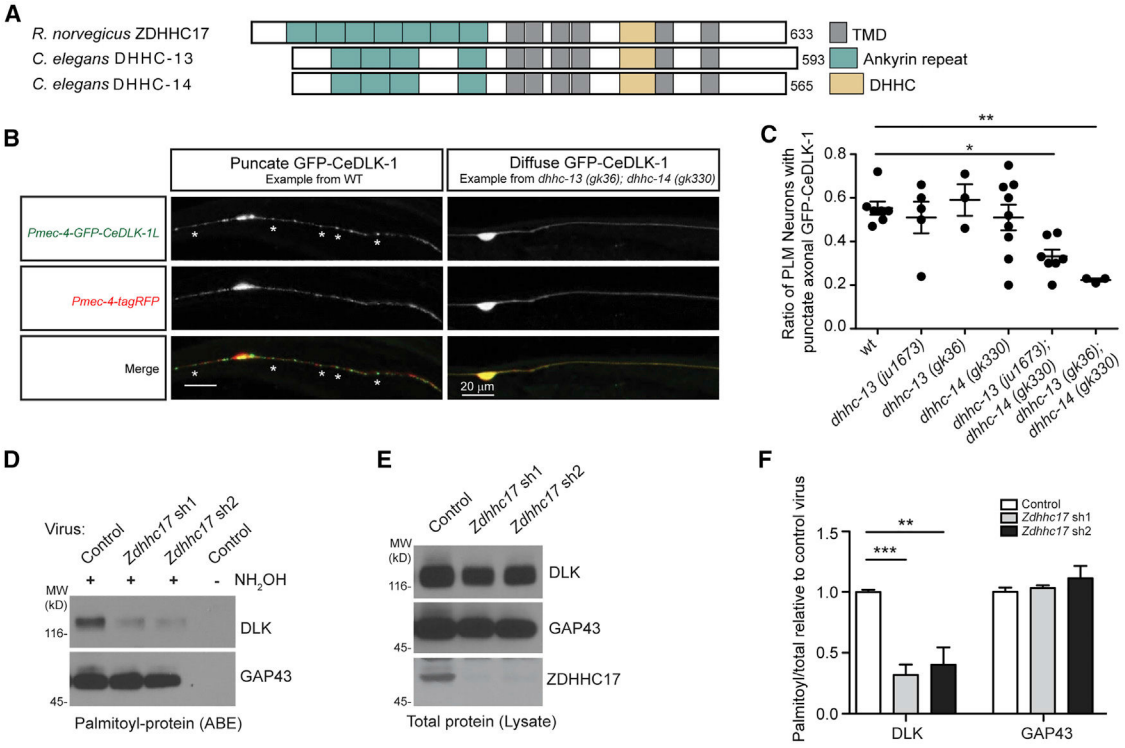

Figure 2. ZDHHC17 Controls DLK Palmitoylation

(A) Alignment of Rat ZDHHC17 with Ce-DHHC-13 and Ce-DHHC-14, showing ankyrin repeats, transmembrane domains (TMDs), and DHHC domain.

(B) Images of GFP-tagged CeDLK-1 (GFP-CeDLK-1) and cell fill tagRFP from WT and *dhhc-13;dhhc-14* mutant worm sensory neurons. Bottom: merged GFP-CeDLK-1 and TagRFP signals are shown. Asterisks highlight punctate GFP-CeDLK-1.

(C) *Ce dhhc-13;dhhc-14* double mutants show reduced punctate GFP-CeDLK-1 localization. Each data point represents the ratio of PLM with punctate GFP-CeDLK-1 to total, from an independent group of 30–70 animals. $^{**}p < 0.01$; $^{*}p < 0.05$; one-way ANOVA.

(D and E) Western blots of ABE and total lysate samples from DRG neurons infected with the indicated lentiviruses. *Zdhhc17* shRNA knockdown reduces palmitoylation of DLK, but not GAP43. Parallel ABE assays omitting hydroxylamine (NH_2OH) lack palmitoyl-protein signal.

(F) Palmitoyl:total DLK and GAP43 from (D) and (E); n = 5; $^{***}p < 0.001$; $^{**}p < 0.01$; one-way ANOVA; Bonferroni post hoc test.

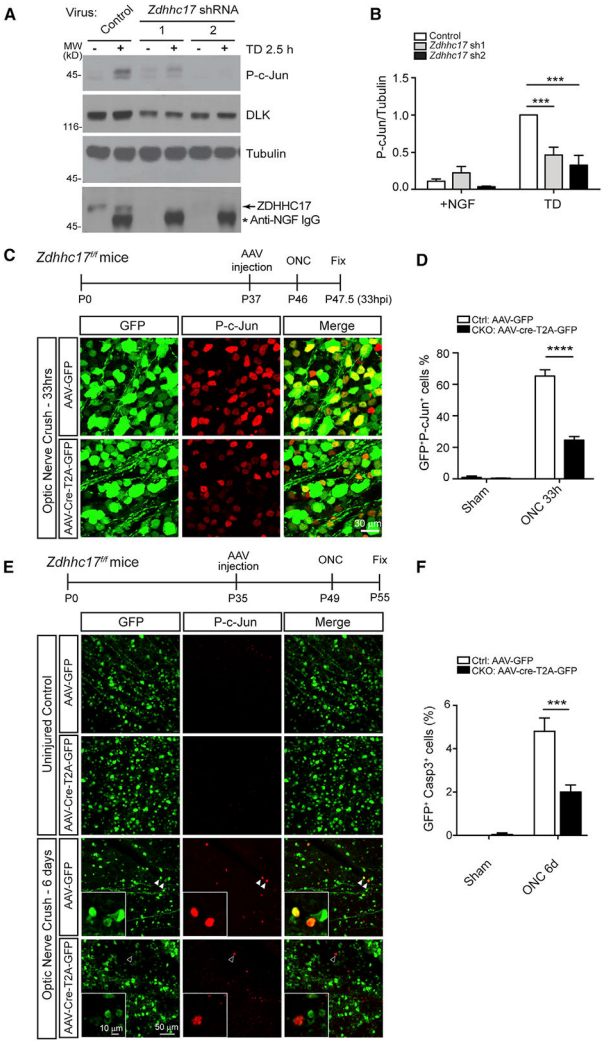

Figure 3. ZDHHC17 Controls DLK Signaling

(A) Cultured DRG neurons infected with the indicated lentiviruses were subjected to TD for 2.5 h or left unstimulated and then lysed and blotted as indicated. Lower panel shows ZDHHC17 (arrow) and anti-NGF antibody used for TD, detected by secondary antibody (asterisk).

(B) Quantified data from (A); n = 5; ***p < 0.001; two-way ANOVA; Bonferroni post hoc test (virus p = 0.0003; TD p < 0.0001; interaction p = 0.0003).

(C) *Zdhhc17* CKO blocks DLK-dependent signaling. Top: experimental setup is shown. Bottom: immunostained retinal flat mounts from *Zdhhc17*$^{f/f}$ mice injected with the indicated AAVs and fixed 33 h post-ONC are shown. Right panels: overlay of columns 1 to 2 are shown.

(D) Quantified GFP^{+}/p-c-Jun^{+} cells from (C). ***p < 0.001; two-way ANOVA; Bonferroni post hoc test; n = 4 (virus p < 0.0001; ONC p < 0.0001; interaction p< 0.0001).

(E) *Zdhhc17* CKO blocks ONC-induced caspase-3 (Casp3) activation. Top: experimental setup is shown. Bottom: immunostained retinal flat mounts from *Zdhhc17*$^{f/f}$ mice injected with the indicated AAVs and fixed 6 days post-ONC are shown. Right panels: overlay of

columns 1 to 2 is shown. Filled arrowheads, GFP/Casp3 double-positive RGC; empty arrowhead, GFP-positive/Casp3-negative RGC. Insets, magnified images of cells highlighted by arrowheads.

(F) $GFP^+/Casp3^+$ cells from (E); n = 5–6. ***p < 0.001; two-way ANOVA; Bonferroni post hoc test. n = 5–6 (virus p = 0.0013; ONC p < 0.0001; interaction p = 0.0009).

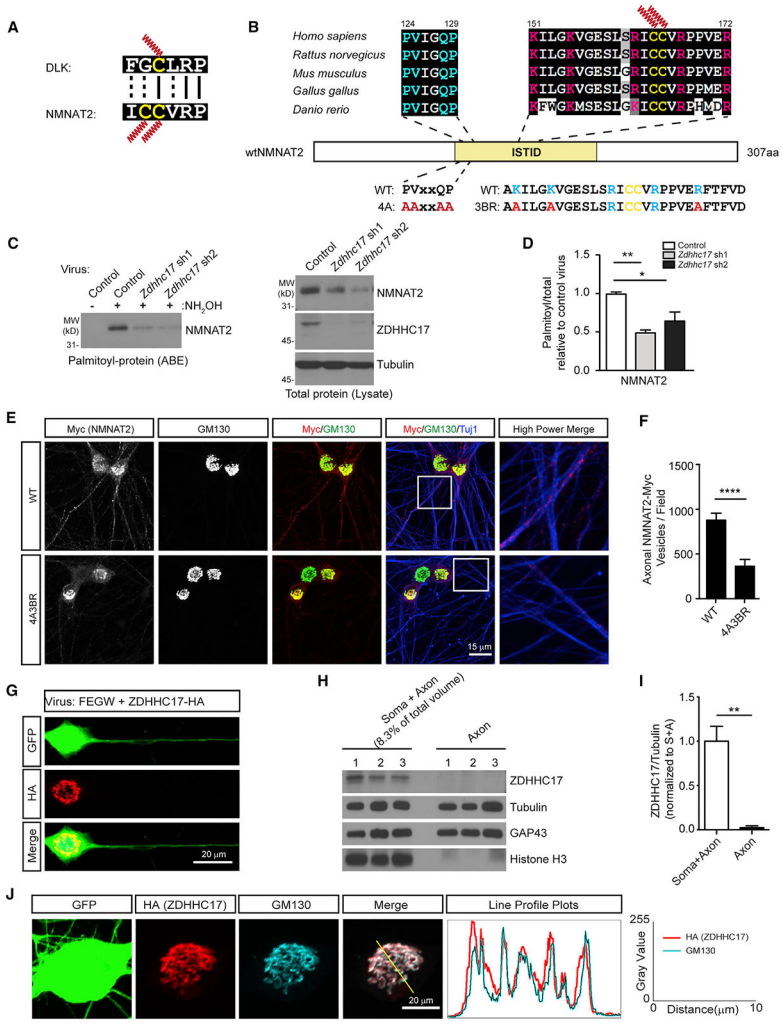

Figure 4. DLK and NMNAT2 Palmitoyl Sites Are Homologous, and NMNAT2 Palmitoylation and Localization Are ZDHHC17 Dependent

(A) Sequences around DLK (top) and NMNAT2 palmitoyl sites (bottom).

(B) NMNAT2's isoform-specific targeting and interaction domain (ISTID) (yellow) contains zDABM consensus (cyan), basic residues (BRs) (important for membrane binding and palmitoylation; Milde et al., 2013; magenta), and palmitoyl-cysteines (yellow). Residues mutated in NMNAT2-4A, -3BR, and -4A-3BR mutants are shown below.

(C) Western blots of ABE and total lysate samples from DRG neurons infected with the indicated lentiviruses.

(D) Quantified data from (C); n = 5. **p < 0.01; *p < 0.05; one-way ANOVA; Bonferroni post hoc test.

(E) DRG neurons lentivirally infected to express myc-tagged NMNAT2-WT or 4A-3BR mutant, immunostained as indicated. 5th column, magnified view of boxed area in 4th column.

(F) Quantified data from (E) confirm reduced axonal targeting of NMNAT2-4A-3BR. ****p < 0.0001; t test.

(G) Immunostained cultured DRG neurons coinfected with the indicated lentiviruses. Images are representative of 10 individual neurons.
(H) Western blots of somata plus axons (soma + axon) or distal axons only (“axon”) fractions from 3 sets of DRG neuron microfluidic cultures.
(I) Quantified data from (H); n = 4. **p < 0.01; t test.
(J) DRG neurons infected as in (G) and immunostained as indicated. Right: somal line profile (yellow in merged image) confirms overlapping HA-ZDHHC17 and GM130 signals.

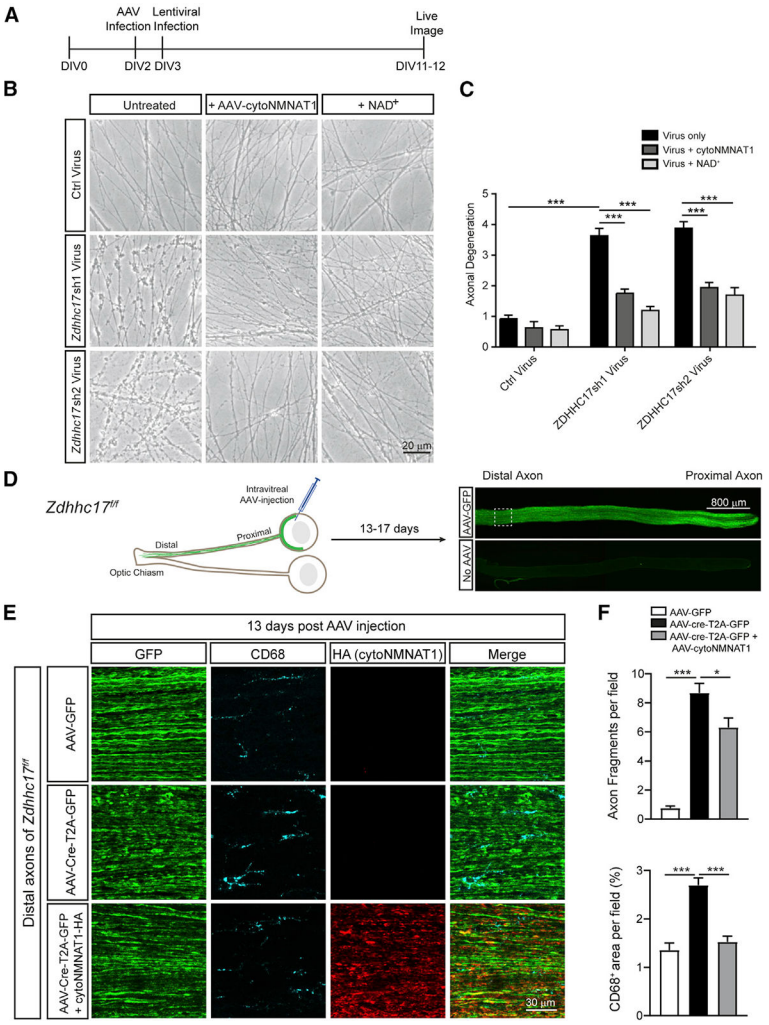

Figure 5. Prolonged *Zdhhc17* Loss Triggers NMNAT-Dependent Distal Axon Degeneration

(A) Experimental setup. Subsets of DRG cultures were infected with AAV expressing CytoNMNAT1-HA or fed every 2 days with 1 mM NAD^+.

(B) Images of distal axons from cultures infected and/or treated as in (A).

(C) Quantified data from (B); n = 3; ***p < 0.001, n.s., not significant. One-way ANOVA; Bonferroni post hoc test.

(D) Left: experimental setup. Right: anti-GFP immunostaining of optic nerve sections from eyes intravitreally injected with AAV-GFP (top) or uninjected ("no AAV," bottom). Red box, approximate region imaged in later panels. Scale bar: 800 μm.

(E) Immunostained optic nerves from *Zdhhc17*$^{f/f}$ mice intravitreally injected with the indicated AAVs and fixed 13 days later.

(F) Quantified data from (E). ***p < 0.001; *p < 0.05; one-way ANOVA; post hoc Bonferroni test; n = 4–8.

KEY RESOURCES TABLE

REAGENT or RESOURCE	SOURCE	IDENTIFIER
Antibodies		
Rabbit anti-phospho c-Jun S63 II	Cell Signaling Technology	Catalog # 9261, RRID: AB_2130162
Rabbit anti-phospho c-Jun S73	Cell Signaling Technology	Catalog # 3270, RRID: AB_2129575
Rabbit anti-phospho c-Jun S63	Cell Signaling Technology	Catalog # 91952
Rabbit anti-DLK/MAP3K12	Sigma/ Prestige	Catalog# HPA039936, RRID: AB_10795239
Rabbit anti-DLK/MAP3K12	Thermofisher Scientific	Catalog# PA5-32173, RRID: AB_2549646
Mouse anti-GFP	Life Technologies	Catalog# A11120, RRID: AB_221568
Rabbit anti-GFP	Life Technologies	Catalog # A11122, RRID: AB_221569
Mouse anti-Tubulin β3	BioLegend/Covance	Catalog # MMS-435P, RRID: AB_2313773
Mouse anti-Myc 9E10	UPenn Cell Center	Catalog #3207
Mouse anti-Myc 9E10	Enzo Life Sciences	Catalog#: ENZ-ABS463-0200
Rabbit anti-Myc	Cell Signaling Technology	Catalog # 2278, RRID: AB_490778
Mouse anti-HA11	BioLegend	Catalog # 901502, RRID: AB_2565007
Rabbit anti HA	Cell Signaling Technology	Catalog #3274, RRID: AB_1549585
Mouse anti-tubulin	Millipore Sigma	Catalog # T7451, RRID: AB_609894
Sheep anti-NGF	CedarLane	Catalog # CLMCNET-031, RRID: AB_10060173
Rabbit anti-RBPMS	Millipore Sigma	Catalog# SAB2101964, RRID: AB_2687403
Rabbit anti-ZDHHC17	Millipore Sigma	Catalog # H4714, RRID: AB_1858997
Mouse anti-Brn3a	Millipore Sigma	Catalog # MAB1585, RRID: AB_94166
Rat anti-CD68	Bio-Rad	Catalog # MCA341GA RRID: AB_323909
Rabbit anti-GAP43	Novus	Catalog # NB300-143, RRID: AB_10001196
Mouse anti-NMNAT2 (B-10)	Santa Cruz Biotechnology	Catalog # sc-515206, RRID: AB_2827765
Mouse anti-GM130	BD Biosciences	Catalog # 610822, RRID: AB_398141
Mouse anti-histone H3	Cell Signaling Technology	Catalog # 4499, RRID: AB_10544537
Rabbit anti-Cleaved Caspase-3	Cell Signaling Technology	Catalog # 9661, RRID: AB_2341188
Bacterial and Virus Strains		
Stbl3 *E.coli*	Thermofisher	Catalog #737303
VSV-G pseudotyped lentivirus (pFUW backbone vector)	Lois et al., 2002	N/A
pFEGW lentivirus (backbone vector modified from pFUW)	Holland et al., 2016	N/A
pFEGW DLKsh lentivirus	Holland et al., 2016	N/A
pFEW wtDLK-myc lentivirus (shRNA resistant)	Holland et al., 2016	N/A
pFEW DLK-CS-myc lentivirus (shRNA resistant)	Holland et al., 2016	N/A

REAGENT or RESOURCE	SOURCE	IDENTIFIER
pFEW HA-Zdhhc17 lentivirus	This study	N/A
pFEW Zdhhc17-HA lentivirus	This study	N/A
pFEW wtNMNAT2-myc lentivirus	This study	N/A
pFEW NMNAT2-4A3BR-myc lentivirus	This study	N/A
pAAV-GFP adeno-associated virus	This study	N/A
pAAV-GFP-DLKsh adeno-associated virus	This study	N/A
pAAV-Cre-T2A-GFP adeno-associated virus	This study	N/A
pAAV-wtDLK-HA adeno-associated virus (shRNA resistant)	This study	N/A
pAAV-DLK-CS-HA adeno-associated virus (shRNA resistant)	This study	N/A
pAAV-cytoNMNAT1-HA adeno-associated virus	This study	N/A
Biological Samples		
DRG neurons, cultured from E16 Sprague Dawley rat	Holland et al., 2016	N/A
Chemicals, Peptides, and Recombinant Proteins		
Nerve Growth Factor	Alomone Labs	Catalog # N-100
Biotin-HPDP	Soltec Ventures	Catalog # B106
β-Nicotinamide adenine dinucleotide hydrate (NAD+)	Millipore Sigma	Catalog # N1636
Cas9-NLS purified protein	QB3 MacroLab, UC Berkeley	N/A
Deposited Data		
Mouse single cell RNA-seq data	http://www.mousebrain.org, Zeisel et al., 2018	N/A
Experimental Models: Cell Lines		
Human: Human Embryonic Kidney (HEK) 293T cells	ATCC	CVCL_0063
AAVpro® 293T Cell Line	Takara Bio	Catalog # 632273
Experimental Models: Organisms/Strains		
Embryonic neurons from rat, Sprague-Dawley	Charles River	Strain code 400
Mouse, C57BL/6	Jackson Labs	Strain code 000664
Mouse: *Zdhhc17*$^{fl/fl}$ in FVB background strain	Sanders et al., 2016	N/A
C. elegans: CZ23498 *[Pmec-4-GFP::DLK-1L, Pmec-4-tagRFP](juIs501).*	Noma and Jin, 2018	CZ23498
C. elegans: CZ26344 *dhhc-13(gk36) IV; [Pmec-4-GFP::DLK-1L, Pmec-4-tagRFP] (juIs501).*	This paper	CZ26344
C. elegans: CZ26345 *dhhc-14(gk330) X; [Pmec-4-GFP::DLK-1L, Pmec-4-tagRFP] (juIs501).*	This paper	CZ26345
C. elegans: CZ26346 *dhhc-13(gk36) IV; dhhc-14(gk330) X; [Pmec-4-GFP::DLK-1L, Pmec-4-tagRFP](juIs501).*	This paper	CZ26346
C. elegans: CZ26965 *dhhc-13(ju1673) IV; [Pmec-4-GFP::DLK-1L, Pmec-4-tagRFP] (juIs501).*	This paper	CZ26965
C. elegans: CZ26966 *dhhc-13(ju1673) IV; dhhc-14(gk330) X; [Pmec-4-GFP::DLK-1L, Pmec-4-tagRFP](juIs501).*	This paper	CZ26966
Oligonucleotides		
Please refer to Table S1 for sequences, sources and identifiers of oligonucleotides used in this study		N/A

REAGENT or RESOURCE	SOURCE	IDENTIFIER
Recombinant DNA		
pAAV-GFP	This study	N/A
pAAV-GFP-DLKsh	This study	N/A
pAAV-Cre-T2A-GFP	This study	N/A
pAAV-wtDLK-HA (shRNA-resistant)	This study	N/A
pAAV-DLK-CS-HA (shRNA-resistant)	This study	N/A
pAAV-cytoNMNAT1-HA	This study	N/A
pAAV2 (pACG2)-RC triple mutant	Petrs-Silva et al., 2011	N/A
pHelper	Agilent	N/A
pFEGW	Holland et al., 2016	N/A
pFEGW DLKsh	Holland et al., 2016	N/A
pFEW wtDLK-myc (shRNA-resistant)	Holland et al., 2016	N/A
pFEW DLK-CS-myc (shRNA-resistant)	Holland et al., 2016	N/A
wtDLK in pEGFP-N1	Holland et al., 2016	N/A
DLK-CS in pEGFP-N1	Holland et al., 2016	N/A
DLK-PVAA in pEGFP-N1	This study	N/A
pFEW HA-Zdhhc3	This study	N/A
pFEW HA-Zdhhc5	This study	N/A
pFEW HA-Zdhhc10	This study	N/A
pFEW HA-Zdhhc14	This study	N/A
pFEW HA-Zdhhc15	This study	N/A
pFEW HA-Zdhhc17	This study	N/A
pFEW Zdhhc17-HA	This study	N/A
pFEW Zdhhc17-N100A-HA	This study	N/A
wtNMNAT2 in pEGFP-N1	This study	N/A
pFEW wtNMNAT2-myc	This study	N/A
pFEW NMNAT2-4A-myc	This study	N/A
pFEW NMNAT2-3BR-myc	This study	N/A
pFEW NMNAT2-4A3BR-myc	This study	N/A
Plasmid: pCZGY2333 *Pmec-4*-tagRFP	Holland et al., 2016	pCZGY2333
Plasmid: pCZGY2335 *Pmec-4*-GFP::DLK-1L-3′ UTR(*let-858*)	Holland et al., 2016	pCZGY2335
Software and Algorithms		
NIH ImageJ	NIH Image	SCR_003070
Fiji	Laboratory for Optical and Computational Instrumentation	SCR_002285
GraphPad Prism	GraphPad Software Inc.	SCR_002798